SEA SURFACE TEMPERATURES IN THE BAY OF BENGAL THROUGH THE PLIOCENE-PLEISTOCENE CLIMATE TRANSITION

A Thesis submitted to the faculty of
San Francisco State University
In partial fulfillment of
the requirements for
the Degree

Master of Science

In

Geoscience

by

Kara Susan Cowan

San Francisco, California

January 2021

CERTIFICATION OF APPROVAL

I certify that I have read Sea Surface Temperatures in the Bay of Bengal through the Pliocene-Pleistocene climate transition by Kara Susan Cowan, and that in my opinion this work meets the criteria for approving a thesis submitted in partial fulfillment of the requirement for the degree Master of Science in Geoscience at San Francisco State University.

Petra S. Dekens, Ph.D.
Professor,
Thesis Committee Chair / Date

Brendan Reilly, Ph.D.
Postdoctoral Scholar, UCSD / Date

Alexander Stine, Ph.D.
Associate Professor / Date

SEA SURFACE TEMPERATURES IN THE BAY OF BENGAL THROUGH THE PLIOCENE-PLEISTOCENE CLIMATE TRANSITION

Kara Susan Cowan
San Francisco, California
2021

The Pliocene-Pleistocene climate transition is characterized with a global cooling trend and increased glacial-interglacials. During this climate transition sea surface temperatures (SST) in the Indo-Pacific Warm Pool (IPWP) remained stable, while SST in the eastern equatorial Pacific cooled 1-2°C. There are few SST records in the Indian Ocean regions that link the IPWP to the areas with strong monsoon variations. We reconstructed paleoclimate conditions through the Pliocene-Pleistocene climate transition in the Bay of Bengal at IODP Site 1451A (8°N, 88°E in 3607 m water depth). We used the Mg/Ca of *T. sacculifer* to establish a SST record that maintained stability with a trend of ~0.6°C that is statistically insignificant. We refined the Site U1451A age model by comparing the Site U1451A *U. peregrina* benthic $\delta^{18}O$ record to the global benthic $\delta^{18}O$ record (the LR04 stack). The refined age model defined gives the time interval of ~2.1-3 Ma with an uncertainty of $\pm$20 kyr.

ACKNOWLEDGEMENTS

I would like to thank my advisor, Dr. Petra Dekens, and my committee members, Dr. Brendan Reilly and Dr. Alexander Stine, for their insight and guidance to this study. I would like to thank all of the scientists on the IODP Expedition 354 cruise for their work to make this study and many others possible. I would also like to thank the UC Santa Cruz Stable Isotope Laboratory for the analysis during the start of the COVID-19 pandemic. Additionally, I would like to thank Dr. Christina Ravelo and her laboratory at UC Santa Cruz for laboratory assistance. I would like to thank the SFSU CoSE travel grant and the Pestrong Grant for their funding for national and regional conferences. I would like to thank the members and students of the department at San Francisco State University for their scientific collaboration. Finally, I would like to thank my family and close friends that have supported me unconditionally throughout the process of my master's thesis.

TABLE OF CONTENTS

LIST OF TABLES

LIST OF FIGURES

Figures Page

LIST OF APPENDICES

INTRODUCTION

During the Pliocene to Pleistocene (2-3 Ma) climate transition the Earth gradually cooled from a time of relative global warmth in the early Pliocene to cooler conditions that include the onset of significant Northern Hemisphere glaciation (NHG) and increased glacial-interglacial amplitude (Lisiecki & Raymo, 2007). The early Pliocene (4 to 5 Ma) is characterized by globally warmer temperatures (Dekens et al., 2008; Fedorov et al., 2013) and little ice in the northern hemisphere. The Pliocene-Pleistocene (2 to 3 Ma) transition includes a gradual cooling, which is observed in the trend toward heavier benthic $\delta^{18}O$ data in the global record (LR04 stack; Lisiecki & Raymo, 2005), and by an increase in glaciation in the northern hemisphere, which is recorded by the increased deposition of ice rafted debris (IRD; Kleiven et al., 2002). The IRD indicates that although there was some ice present in the Northern Hemisphere in the late Miocene (St John & Krissek, 2002), there was a marked increase in IRD in the North Pacific and North Atlantic at ~3 Ma (Maslin et al., 1996; Kleiven et al., 2002). At ~2.75 Ma, regions across the Northern Hemisphere all experienced peak pulses in IRD records that occurred synchronously, marking the onset of significant NHG (Maslin et al., 1996; Kleiven et al., 2002). The increase in total ice volume was accompanied by increased glacial-interglacial amplitudes (Lisiecki & Raymo, 2005). Both the IRD and benthic $\delta^{18}O$ records record conditions at high latitudes and broad changes in the global climate.

It is important to understand how the Pliocene-Pleistocene transition manifested in the world's tropical oceans, as the sea surface temperatures (SST) in these regions have a large control on climate through ocean atmosphere feedbacks. In today's climate, the EEP cold tongue

has SST's about ~5°C cooler than the western equatorial Pacific (WEP; Figure 1; Levitus, 1982). The SST difference between the EEP and WEP generates the zonal overturning atmospheric circulation of the Walker Cell, which strengthens the trade winds and causes further cooling of the EEP through equatorial divergent upwelling (Lindzen & Nigam, 1987). When this SST gradient disappears during an El Nino event, there are global impacts on climate (i.e., drought in Australia, floods in parts of South America, reduced hurricanes, and globally warmer temperature).

The early Pliocene (~4-5 Ma) is the most recent time of global warmth. During this time, warm SST, which are predominantly constrained to the western sides of the tropical oceans today, extended much past the equator into the mid latitudes and reduced the meridional SST gradient (Fedorov et al., 2013). The very warm SST seen in the Indo-Pacific warm pool (IPWP) today (29°C) also extended into the eastern equatorial Pacific (EEP). The EEP began cooling in the Pliocene and continued cooling through the Pleistocene (Wara et al., 2005; Lawrence et al., 2006). During the Pliocene-Pleistocene transition the EEP cooled by 1 to 2°C (Lawrence et al., 2006; Wara et al., 2005; Seki et al., 2012; Dekens et al., 2007). The IPWP remained relatively unchanged over the last 5 Ma while much of the global ocean cooled during the Pliocene-Pleistocene transition (Wara et al., 2005; Fedorov et al., 2013; Dekens, unpublished). The EEP (alkenone analysis from ODP 846 at 3°S) and WEP (Mg/Ca analysis from ODP 806 at 0°N) temperature difference increased from 2.4°C at 3.1 Ma to 3.5°C at 2.3 Ma, which demonstrates that the modern zonal SST gradient began to form during the Pliocene-Pleistocene transition (Medina-Elizalde & Lea, 2010).

The Bay of Bengal in the Indian Ocean is influenced by the IPWP and the Indian summer monsoon. The southern part of the Bay of Bengal has very warm SST (~29°C) that are similar to the IPWP (Figure 1; Levitus, 1982). However, the northern Bay of Bengal is more directly influenced by the Indian summer monsoon, and the increased rainfall over the summer months on this region contributes to the lower salinity in the northern Bay of Bengal (Levitus, 1982). The seasonal current, Southwest Monsoon Current (SMC), brings warm water from the southwest into the Bay of Bengal during the summer months (Figure 2). The southern Bay of Bengal lies between the northern Bay of Bengal and the IPWP, making it the link between the monsoon signal and the changing ocean currents that bring the warm water north into the Bay of Bengal. The Indian Ocean is limited to 3 paleoceanographic records (ODP sites 722, 709, and 214) over the Pliocene-Pleistocene climate evolution. ODP site 722 (17°N, 60°E) is in an upwelling region in the Arabian Sea with lower SST that are not representative of the typical IPWP waters (Herbert et al., 2010). ODP sites 709 (3°S, 60°E) and 214 (11°S, 88°E) are sites in the IPWP that have records during this climate evolution but are not in the heavily monsoon influenced region of the Bay of Bengal. Of these 3 paleoceanographic sites, none of these records can provide the link of monsoon variability with the Indo-Pacific warm pool regions. Generating a SST record in the Bay of Bengal will help us better understand the links between tropical SST dynamics of the IPWP and the monsoon during the Pliocene-Pleistocene transition.

BACKGROUND

Bay of Bengal

The Bay of Bengal is a unique region where the Himalayan mountain range, the Tibetan plateau, and the Asian Monsoon system all interact to influence climate. The Tibetan plateau started to grow at ~50 Ma after India collided with Eurasia and has uplifted to reach the present-day height of 5 km (Molnar et al., 2010; Zhisheng et al., 2015). This dominant feature in Asian topography was thought to be the primary heat source that drives the Asian monsoon system (Li & Yanai, 1996), but recent models have shown that the Indian summer monsoon would be present with the removal of the Tibetan plateau as long as the Himalayan mountain range remained (Boos & Kuang, 2010). The Himalayan mountain range contributes to the strong Indian summer monsoon by isolating warm and moist air over India from the cold and dry mid latitudes (Boos & Kuang, 2010). While the atmospheric models show that the Tibetan plateau is not important for the Indian summer monsoon, the plateau heating is related to increased rainfall into the Himalayas (Boos & Kuang, 2010).

The Himalayan mountain range acts as an orographic barrier and is the source of most of the sediment from the Ganges-Brahmaputra river system that drains into the Bay of Bengal via turbidity currents and results in the world's largest fan system (Weber et al., 1997; Curray et al., 2003; France-Lanord et al., 2016). The Ganges and Brahmaputra river sediments have a dominant clay mineral composition of illite, mainly a weathering product of lithic material from the Himalayas, and a secondary composition of smectite (~23%) which comes mainly from the Ganges river (Roonwal et al., 1997; Khan et al., 2019). Sediments transported via turbidity currents to the Bengal fan are mainly terrigenous with the exception of calcareous sediments ($CaCO_3$ content reaches 75%) near the Ninetyeast Ridge (Kolla et al., 1976; Roonwal et al., 1997; Curray et al., 2003). During low sea level conditions, rapid sediment deposition occurs and

generates huge turbidity currents that fill the upper fan channels and move through the channel-levee system (Curray et al., 2003). The turbidity currents spill over the levees as lateral sheet flow and is carried down the channel with turbidity current deposition occurring at the lower Bengal fan (Curray et al., 2003). The turbidity currents make this region difficult to obtain paleoceanographic records, but the large summer monsoon make it important to find links within the climate system.

The land-air-sea dynamics that create the Indian monsoon are shown through the pressure gradients and seasonal reversal of wind direction that is accompanied by the reversal of surface currents (Schott & McCreary, 2001). Monsoon circulation is associated with the variation of large-scale pressure gradients in various monsoon regions (Zhisheng et al., 2015). The associated surface climate to the monsoon is characterized by a seasonal reversal of prevailing wind direction and a seasonal alternation of dry and wet conditions (Zhisheng et al., 2015). The productivity and wind strength signals in the northern Arabian Sea are mainly controlled by Indian summer monsoon processes (Clemens et al., 2010; Ziegler et al., 2010; Caley et al., 2011). During the summer months, the SMC flows eastward south of Sri Lanka and then turns northward to bring saltier Arabian Sea water into the Bay of Bengal (Jensen, 2003). During the summer monsoon season, the West Indian Coastal Current flows south and connects with the SMC to carry high-salinity waters eastward into the southern Bay of Bengal (Figure 2; Schott and McCreary, 2001; Schott et al., 2009).

The surface salinity in the northern Bay of Bengal is influenced by direct rainfall over the ocean and by increased freshwater flux discharged from the Ganges-Brahmaputra river system

(Clemens et al., 2016). The Indian summer monsoon accounts for a combined Ganges-Brahmaputra water discharge of ~1.7 x 10^5 m^3/s, from a non-monsoon winter base level of ~0.2 x 10^5 m^3/s (Singh et al., 2008). The impact of the summer monsoon is seen in the salinity of the northern Bay of Bengal which has a seasonal range of ~27-31 while the southern Bay of Bengal has a seasonal range of ~33-34 (Figure 2; Levitus, 1982). The SST variability in the northern Bay of Bengal has a seasonal range of ~25-30°C while the southern Bay of Bengal has a seasonal range of ~27-30°C (Figure 2; Levitus, 1982). The rainfall and the discharge from the river system result in the northern Bay of Bengal having the strongest monsoon signal in both seasonal salinity stratification variability and SST variability (Li et al., 2017).

IODP Expeditions 353 and 354 set out to build an understanding of how this important region, where the summer monsoon impacts the climate variability in the Bay of Bengal region, has changed through the last 50 Ma. Expedition 353 drilled sites in the northern Bay of Bengal to obtain records that give a direct signal from the Indian Monsoon (Clemens et al., 2016). Expedition 354 drilled seven sites along an east-west transect at 8°N in the southern Bay of Bengal (Figure 3; France-Lanord et al., 2016).

Foraminifera as paleoclimate archives

We used foraminifera to reconstruct SST in the southern Bay of Bengal to gain a better understanding of the transition from the Pliocene to the Pleistocene in this region. The calcite shells of foraminifera reflect the ocean chemistry of their depth habitats and are frequently used to reconstruct paleoceanographic conditions. Mg is a conservative element, and the Mg/Ca of

seawater does not vary with depth in the water column (Broecker and Peng, 1982). The substitution of Mg in calcite is a thermodynamic process in which the Mg/Ca content increases exponentially by about ~3% per degree between 0°C and 30°C (Koziol and Newton, 1995). Planktonic foraminifera show a clear exponential relationship between the Mg/Ca ratios and temperature of the water in which they precipitated their shell, which is the basis using Mg/Ca of foraminifera shells as a paleotemperature proxy (Nürnberg et al., 1996; Lea et al., 1999; Dekens et al., 2002; Anand et al., 2003; Regenberg et al., 2006).

Three main approaches have been used to establish the relationship between Mg/Ca in planktonic foraminifera and the temperature of the water in which they calcify their shells: laboratory culturing, sediment traps, and sediment core top studies. Laboratory culturing of foraminifera create controlled conditions to reveal the relationship between Mg content in foraminifera tests and variable temperatures (Lea et al., 1999; Kisakurek et al., 2008). A laboratory culture study based on the planktonic species of foraminifera, *G. sacculifer*, resulted in 130% magnesium concentration increase when the temperature increased by 10°C (Nürnberg et al., 1996). Sediment trap time series data is collected using foraminifera from the water column with the advantage of obtaining seasonal and interannual records and have been used to define the sensitivity of calcite foraminifera Mg/Ca to calcification temperature as a 9% change in Mg/Ca for a 1°C change in temperature (Anand et al., 2003). Core top studies have confirmed this relationship by comparing Mg/Ca of planktonic foraminifera in core tops to modern SST in the overlying water column (Dekens et al., 2002; Regenberg et al., 2006). However, core tops from different ocean depths also demonstrate that the Mg/Ca of planktonic foraminiferal calcite decreases with increasing water depth as a result of dissolution (Rosenthal and Boyle, 1993;

Dekens et al., 2002; Regenberg et al., 2006). The preferential removal of Mg in calcite due to dissolution significantly alters the Mg/Ca temperature proxy that is essential for a reliable reconstruction (Brown and Elderfield, 1996). Multiple studies have created methods to correct for dissolution when constructing calibrations for the Mg/Ca proxy (Dekens et al., 2002; Regenberg et al., 2006). The ΔCO_3^{2-} ion is the main control on calcite dissolution within the water column and at the sediment-water interface, allowing it to be used as a parameter for the correction of Mg/Ca dissolution (Dekens et al., 2002).

Trace metals contaminants can also influence the Mg/Ca of calcite foraminifera calcite. Mn-overcoating can also alter the Mg/Ca proxy because manganese carbonate can contain high levels of other trace elements (including Mg) that alters the foraminifera shell composition (Boyle, 1983). Comparison of Mn/Ca in core tops, sediment traps and deep-sea sediments has shown higher Mn/Ca values due to the formation of manganese carbonate overgrowths (Boyle, 1983). In order to use the deep-sea samples, reductive cleaning steps are needed to remove the Mn-rich coatings (Barker et al., 2003). Work from Emiliani (1955), first suggested that the Mg content measured in foraminiferal calcite, that records temperature conditions, is also associated with silicate contamination and washing the specimens is not enough to limit the bias before analysis. Silicate contamination alters the Mg/Ca of foraminifera and the removal of silicate contamination is the most important step for the measurement of Mg/Ca ratios (Barker et al., 2003).

The measurement of the $\delta^{18}O$ of the calcite of benthic foraminiferal species have been used as a paleoclimate proxy for temperature and global ice volume. The global nature of the ice

volume signal allows the $\delta^{18}O$ proxy to be used to place marine sediment records on a common timescale (Lisiecki & Raymo, 2005; Lisiecki & Stern, 2016). At the same oceanic location coexisting benthic foraminiferal species often have different $\delta^{18}O$ due to whether or not the species calcifies their shell in equilibrium with seawater (Duplessy et al., 1970). The benthic species *C. wuellerstorfi* is suggested to calcify in equilibrium with seawater, while *U. peregrina* (this study) is suggested to not calcify in equilibrium with seawater (Bemis et al., 1998). Other factors that influence benthic $\delta^{18}O$ are kinetic fractionation effects, metabolic fractionation effects, and preservation effects (Hoogakker et al., 2010). Therefore, an important assumption made in paleoceanographic studies is that the offset between $\delta^{18}O$ of coexisting benthic foraminiferal species is constant (Hoogakker et al., 2010) and this allows us to use the $\delta^{18}O$ stable isotope of benthic foraminifera to develop an age model for this study.

METHODS

IODP Site U1451A is the easternmost site of the seven-site transect located north of the western flank of the Ninetyeast Ridge (8°0.42'N, 88°44.50'E in 3607.3 m water depth) on the Bengal Fan at 8°N (France-Lanord et al., 2016). Shipboard biostratigraphy and magnetic reversals placed Cores U1451A-23H and 24H around the Pliocene/Pleistocene boundary (France-Lanord et al., 2016). This site is ideal for the Pliocene-Pleistocene climate transition reconstruction due to the location next to the Ninetyeast Ridge and the calcareous clay lithology of Cores 23H and 24H (Figure 4) – a lithology that was demonstrated to be suitable for paleoclimate work in the late Quaternary (e.g., Weber et al., 2018).

Cores 23H and 24H from site U1451A (121.5-138.14 MBSF) were selected to examine paleoceanographic changes across the Pliocene-Pleistocene transition. The cores were sampled (4 cm wide samples) every 10 cm totaling 130 samples. The samples were disaggregated in deionized water, filtered through a 63 μm sieve to remove silt and clay, and then dried in a 40°C oven overnight. Once the samples were dry, the sediment was carefully brushed from the paper funnels into labeled vials. The samples were sieved into specific size fractions and *T. sacculifer* and *U. peregrina* shells were picked from 355-425 μm and 250-355 μm size fractions. 20-30 shells of *T. sacculifer* were picked to ensure a sufficient mass to analyze both Mg/Ca and $\delta^{18}O$. Two shells of *U. peregrina* were picked from 250-355 μm for $\delta^{18}O$ analysis. The planktonic shells were gently cracked open using glass plates and fragments were mixed to create a homogenized sample.

The $\delta^{18}O$ samples were rinsed with MQ with 5 second sonication and then rinsed with methanol to remove clay from the shells. The excess methanol was siphoned away, and samples were left to dry overnight. The $\delta^{18}O$ samples were analyzed by the UC Santa Cruz Stable Isotope Laboratory for $\delta^{18}O_{CO3}$ by acid digestion using an individual vial acid drop Themo Scientific Kiel IV carbonate device interfaced to Thermo Scientific MAT 253 dual-inlet isotope ratio mass spectrometer (iRMS). The samples were loaded into individual vials and dried overnight in a 70°C vacuum oven. All samples were measured with several replicates of the externally calibrated Carrera Marble in-house standard reference material ‘CM12’ and the NBS-18 limestone international standard reference material. Two natural samples of ‘Atlantis II’

powdered coral are run daily as independent quality control to monitor performance. Typical reproducibility of replicate measurements is significantly better than 0.10‰ for $\delta^{18}O_{CO3}$.

The Mg/Ca samples require a more rigorous cleaning process, including both reductive and oxidative steps to remove Mn-overcoating and silicate contamination to decrease the uncertainty in the Mg/Ca temperature proxy. The Mg/Ca samples were first rinsed three times with ultrapure MQ water, twice with methanol, and then three additional MQ rinses. The samples were sonicated 30 seconds during each rinse step. The reductive cleaning step ensured removal of contaminant trace metals, essential for accurate values of the Mg/Ca recording the calcification temperature. We added 100µl of a solution of 10ml ammonium citrate, 10ml ammonium hydroxide, and 1ml 85% anhydrous aqueous hydrazine to each sample. The samples were then closed to prevent outgassing, placed in a hot water bath for 30 minutes, and sonicated for 5 seconds every 2 minutes. The sonication ensured each shell fragment was exposed to the reductive solution (Barker et al., 2003). The reductive solution was removed with 3 ultrapure water rinses and 30 second sonication before beginning the oxidation step. The oxidation step removed organic material by adding 250 µl to each vial of a mixed solution of 50µl 30% hydrogen peroxide and 30ml of 0.1N sodium hydroxide. The samples were then set in a hot water bath for 5 minutes, sonicated for 5 seconds, and then returned to the hot water bath for another 5 minutes. The oxidative solution was then removed with two MQ water rinses and placed in a final hot water bath for 5 minutes with 5 second sonication at the beginning and end. The samples were then transferred to 1.5 ml acid-leached vials using an acid leached 100µl pipette that is rinsed in weak acid and ultra-pure MQ every 5 samples. The samples were then leached with a final weak acid to remove any remaining contaminants. Using a 250µl pipette,

0.001N nitric acid was added to each row of 10 samples and then diluted with MQ water to prevent over dissolution of shell calcite. The acid was siphoned out and the remaining acid was removed with 2 additional rinses of MQ water.

The Mg/Ca samples were measured on an Inductively Coupled Plasma Optical Emission Spectrometer at the University of California, Santa Cruz. To assess instrument precision and accuracy we measured a liquid consistency standard with a known Mg/Ca ratio every 10 samples. The long-term average taken from 47 samples of this standard is 3.32± 0.014 mmol/mol. To assess the repeatability of foraminifera Mg/Ca measurements, we measured standards from a *T. sacculifer* and a *G. crassiformis* species in each set of samples. The long-term values were 2.88± 0.08 mmol/mol and 2.39± 0.1 mmol/mol, respectively.

RESULTS

U. peregrina Stable Isotopes

The $\delta^{18}O$ values of the benthic species *U. peregrina* in Cores U1451A 23H and 24H range from 3.3 to 4.9‰, with a mean of 3.9‰ and a standard deviation of 0.4‰ (Figure 5). The range in $\delta^{18}O$ values increased from Core 24H (3.3 to 4.6‰) to Core 23H (3.4 to 4.9‰). The absolute values in the record differs with the LR04 benthic $\delta^{18}O$ record from 2.09-3 Ma (2.9 to 4.2‰) (Lisiecki & Raymo, 2005), but the range of the U1451A record (1.6‰) is similar to the LR04 record (1.3‰; Figure 6). The LR04 stack is a global record and does not account for the regional differences in the benthic records. ODP site 758 in the Northern Indian Ocean has $\delta^{18}O$ values of

the benthic species *C. wuellerstorfi* that ranges from 2.4-3.9‰ during this time interval (Chen et al., 1995). Comparison of site U1451A's record with ODP site 758 and the LR04 stack is valid based on the assumption that the offset between the $\delta^{18}O$ of different benthic species is constant and explains why the absolute values differ but the ranges are similar in all three (1.3-1.6‰).

Site U1451A Age Model

Shipboard biostratigraphy places Cores 23H and 24H around the Pliocene-Pleistocene boundary (France-Lanord et al., 2016; Reilly et al., 2018). Further work with paleomagnetic measurements indicates that both Cores 23H and 24H contain no magnetic reversals, which implies each section was deposited during a single polarity chron (Reilly et al., 2018). Based on shipboard biostratigraphic data, the sediments were deposited during either the early Matuyama Chron C2r (1.945-2.581 Ma; 0.636 My duration) or late Gauss Chron C2An.1n (2.581-3.032 Ma; 0.451 My duration) (Gradstein et al., 2012; Reilly et al., 2018). Based on the middle Pleistocene hemipelagic calcareous clay sedimentation rates of ~1-2 cm/kyr, it is roughly expected that Core 23H was deposited over 0.396-0.792 My and Core 24H was deposited over 0.341-0.681 My, making it unlikely that both cores were deposited in exclusively Chron C2r or Subchron C2An.1n (Reilly et al., 2018). This suggests that the Gauss-Matuyama magnetic reversal occurred between the bottom of Core 23H and the top of Core 24H, 129.54-131.33 m CSF-A (Reilly et al., 2018). We took the midpoint of the bottom of 23H and the top of 24H (130.6 m) to tie the one magnetic reversal found in this interval to date it at 2.58 Ma (Lisiecki & Raymo, 2005; Reilly et al., 2018). The age model for Site U1451A was constructed by comparing the

$\delta^{18}O$ stable isotope record of the benthic species *U. peregrina* at site U1451A to the global benthic $\delta^{18}O$ stable isotope record and choosing tie points (Figure 6; LR04 stack; Lisiecki & Raymo, 2005). These tie points were selected by aligning the maxima of the interglacials and the minima of the glacials of the LR04 stack (Lisiecki & Raymo, 2005) to the $\delta^{18}O$ benthic record at site U1451A (Figure 6). This strategy is the common practice in paleoceanographic studies instead of aligning the absolute values based on species offsets in $\delta^{18}O$ at the same oceanographic sites. Together, the 7 stratigraphic tie points and the one magnetic reversal combine as the 8 tie points to construct the Site U1451A age model (Figure 7). The tie points were used to calculate sedimentation rates (Table 1; Figure 8), which then were used to convert the depths (121.5-138.14 mbsf) to ages (2.1-3.0 Ma). This age model was one in a series of age models constructed for this site (Appendix 1) using this method to explore possible age-depth combinations.

T. sacculifer Mg/Ca SST estimates

T. Sacculifer Mg/Ca at Site U1451A Cores 23H and 24H has an average value of ~3.45 mmol/mol, and ranges of 2.89 to 4.16 mmol/mol (Figure 9). The Mg/Ca record has a standard deviation of ~0.24 mmol/mol in Core 24H, and ~0.28 mmol/mol in Core 23H. The total standard deviation over the record is ~0.27 mmol/mol. The entire record of Cores 23H through 24H show a slight trend in Mg/Ca of ~0.17 mmol/mol.

We used multiple calibrations to convert the Mg/Ca of *T. sacculifer* to SST (Figure 10). The Anand et al., 2003 calibration used the raw Mg/Ca values for a size fraction and planktonic species conversion which yielded an average SST of ~25.5°C (Figure 9).

> Mg/Ca = B exp(AT) where A and B are constants for ten planktonic species (0.090 and 0.38, respectively).

This is well below the modern average SST in this region (28.5°C). This low SST range may be due to calcite shell dissolution as the sediment trap data used for this calibration came from samples that did not undergo dissolution (Anand et al., 2003). Site U1451A is susceptible to dissolution due to its depth (3607.3 m water depth). To correct for dissolution, we used the approach of Regenberg et al. (2006), which uses the critical calcite saturation state, where Mg^{2+} removal to dissolution starts, and the site-specific ΔCO_3^{2-} ion to obtain the pre-dissolution Mg/Ca value. The Regenberg et al., 2006 calibration was determined by calculating the intersection between the unaffected Mg/Ca means from <2000 m and the regression through the dissolution-affected ratios from >3000 m to determine the onset of dissolution. This provides the critical calcite saturation state ($\Delta_{critical}$) where Mg^{2+}-removal due to dissolution starts (Regenberg et al., 2006).

$Mg/Ca_{initial}$ (Δ-corrected) = $Mg/Ca_{measured} + (\Delta_{critical}-\Delta)/b$

> $\Delta_{critical}$ and b are species-specific (22.10 and 20.87, respectively).
>
> Δ is 0.24.

The Regenberg et al., 2006 Mg/Ca corrected values were then converted to SST estimates using the Anand et al., 2003 calibration, which yielded an average SST ~28.5°C (Figure 10).

Dekens et al., 2002 used ΔCO_3^{2-} and core depth to correct for dissolution in a set of species-specific calibrations. The core depth calibration is built on the premise that core depth is a good proxy for dissolution given that deeper water has lower ΔCO_3^{2-} values. But it must include an offset between the Atlantic and Pacific Ocean basin to account for the different ages of the deep ocean water (older water has lower ΔCO_3^{2-}). There are no Indian Ocean sites used in Dekens et al., 2002 so we applied the Pacific Ocean correction because the deep ocean chemistry of the Indian Ocean is more similar to the Pacific Ocean than the Atlantic.

$$Mg/Ca = 0.37 \exp 0.09 [T- 0.36(\text{core depth km}) – 2.0°C]$$

The dissolution of calcite is controlled by the carbonate chemistry of the water, while core depth is a proxy (Dekens et al., 2002). The Dekens et al., 2002 ΔCO_3^{2-} calibration is based on estimates of ΔCO_3^{2-} of the deep water where the core top samples were collected.

$$Mg/Ca = 0.31 \exp 0.084 [SST + 0.048(\Delta CO_3^{2-})] \qquad \Delta CO_3^{2-} = 0.24 \text{ at this site}$$

The Dekens et al., 2002 ΔCO_3^{2-} calibration yields an average SST ~28.6°C and the core depth calibration yielded an average SST ~28.1°C (Figure 10). The dissolution corrected calibrations using ΔCO_3^{2-} (Dekens et al., 2002; Regenberg et al., 2006) show very similar SSTs (Figure 10; 28.6°C and 28.5°C, respectively).

Dekens et al., 2002 used the ΔCO_3^{2-} at zero (i.e., saturated bottom water) to obtain the preexponential constant in the equation of 0.31. Both Dekens et al., 2002 and Regenberg et al., 2006 approaches use the ΔCO_3^{2-} ion and provide similar SST estimates at Site U1451A. The Dekens et al., 2002 ΔCO_3^{2-} calibration was chosen as the calibration to represent SST at this site (Figure 11) as it can easily be compared to other tropical SST records that also use the Dekens et al., 2002 ΔCO_3^{2-} calibration. The calibration has a standard error estimate of 1.4°C, 95% confidence interval for the preexponential constant is $\pm$0.006, and 95% confidence interval for the exponential constant is $\pm$0.014 (Dekens et al., 2002).

Core 24H has a SST standard deviation of ~0.8°C and Core 23H has a slightly higher standard deviation of ~0.95°C. Linear regression analysis was performed to apply the best fit line to the SST record. There are 82 samples in the SST record and the linear regression analysis yielded the linear trend of $y = 27.15 + 0.5964x_i$ ($R^2 = 0.0351$), which was used to quantify the statistically insignificant cooling trend. The regression analysis was tested at 95% confidence and yielded a P-value of 0.0917 > 0.05, establishing the linear trend insignificant. The slope of the linear trend line gives the change in SST (°C) for every 1 Ma. The age model spanned from ~2.1-3 Ma, resulting in a time span of ~0.9 Ma. Using the age model and the slope of the linear trend, we established that the cooling trend in the SST record from through the Pliocene-Pleistocene transition (~2.1-3 Ma) is ~0.6°C/Myr with a 95% confidence interval of $\pm$ 0.2°C/Myr (Figure 11).

DISCUSSION

Site U1451A Age Model

The series of age models, that were constructed by comparing benthic $\delta^{18}O$ records, were compared to the physical properties L* (sediment lightness) data from Site U1451A (Figure 5) to help determine the most robust age model. The L*, which tracks the relative contribution of biogenic carbonate to lithogenic sediments in Bengal Fan calcareous clays, can be used as an independent check for the age models since it is sensitive to orbital timescale climate variations and, in the middle to late Pleistocene, has lighter colors during interglacial times when $\delta^{18}O$ values were lighter (Weber et al., 2003; 2018; Weber and Reilly, 2018). The L* tuning approach was used for IODP Expedition 354 Site U1452C to establish an age model at orbital resolution in the late Pleistocene in comparison to a suite of other lithologic and geochemical proxies (Weber et al., 2018) and applied to establish age models for all middle to late Pleistocene calcareous clay units drilled during IODP Expedition 354 (Weber and Reilly, 2018).

We compared Core U1451A-23H to 24H L* to the Laskar04 obliquity curve (Laskar et al., 2004) and noted that L* appears to have a 41 kyr cycle at accumulation rates typical for Bengal Fan calcareous clay sediments (i.e., ~2 cm/ka; France-Lanord et al., 2016; Reilly et al., 2020). When the L* data was filtered using a 1/45 = 1/35 kyr^{-1} bandpass filter on the benthic $\delta^{18}O$ constrained age model we note that the L* maxima of Core 23H lined up with times of maximum tilt, while Core 24H did not display as clear of a relationship. However, because we do not know what the phase of the L* signal should be in relation to obliquity, these results

suggest that our inferred accumulation rates are plausible, and we assign an age model uncertainty of ±20 kyr to account for the unknown phase of our record relative to obliquity.

The Site U1451A age model is limited by resolution due to the low abundance of benthic foraminifera found in Cores 23H and 24H. The average resolution obtained from the benthic $\delta^{18}O$ record was ~12 ka, partially due to data gaps in the record from the low abundance of foraminifera. This record is compared to the global benthic $\delta^{18}O$ record (LR04 stack; Lisiecki & Raymo, 2005) which has an average resolution of ~2 ka. The difference in resolution when comparing the U1451A record to the global record brings uncertainty and is the source of the greatest challenge when constructing the age model.

Pliocene-Pleistocene Tropical SST records

The Pliocene-Pleistocene (~2.1-3.0 Ma) SST record for the Southern Bay of Bengal shows no statistically significant trend in the record of ~0.6°C± 0.2°C/Myr (Figure 11). We compared our SST record at Site U1451A to other tropical SST records to help understand the regional impacts of the summer monsoon and the influence of the warm pool on the climate transition (Table 2). The Mg/Ca sea surface temperature (SST) record from ODP 806 in the western equatorial Pacific also does not show a cooling trend during this time period (Medina-Elizalde & Lea, 2010; Wara et al., 2005). A *T. sacculifer* Mg/Ca SST records at IODP site 758 also shows no cooling trend through the last 5 Ma (Dekens, unpublished; Figure 12). The Southern Bay of Bengal (Site U1451A) has an average SST of ~28.6°C which aligns with the

ODP 806 record (Wara et al., 2005) in the WEP and the ODP 758 record (Dekens, unpublished) in the Northern Indian Ocean (Table 2; Figure 12). The similarities in the means between the Southern Bay of Bengal record to the IPWP demonstrates that this is the dominant influence on the Southern Bay of Bengal. Furthermore, the comparison of the Eastern Equatorial Pacific (EEP) (ODP site 847; Wara et al., 2005) with the Southern Bay of Bengal highlights the influence of the warm pool regions on site U1451A. ODP site 847 (Wara et al., 2005) in the EEP cooled with a statistical difference in the mean SST compared to the WEP regions that remained warm and stable (Table 2). The EEP record (Wara et al., 2005) has a wider SST range and is the only region in the tropics known to have cooled during the Pliocene-Pleistocene transition (Table 2). This again highlights that the IPWP remained stable while the EEP cooled during the global cooling trend of the Pliocene-Pleistocene transition.

The Site U1451A age model has allowed the division of Cores 23H (~2.1-2.5 Ma) and 24H (~2.6-3 Ma) into the Pleistocene and Pliocene climate specification, respectively. The standard deviation from the mean reveals the amplitude in the SST record. The analysis of the Pliocene vs the Pleistocene SST record in the Southern Bay of Bengal shows the Pliocene had a SST amplitude of ~0.84°C and a SST amplitude of ~0.95°C in the Pleistocene. This is a very small change in SST amplitude from the Pliocene to the Pleistocene and is statistically insignificant. The comparison of SST variability of the Southern Bay of Bengal to the Northern Indian Ocean (ODP 758; Dekens, unpublished) shows a similar increase in SST variability from the Pliocene (~0.7°C) to the Pleistocene (~1.1°C) (Figure 12).

SUMMARY

The Site U1451A-23H/24H age model was refined from the previous age-depth relationship conversion that used magnetic reversals that were outside the sampling depth range. We refined the age model by comparing Site U1451A *U. peregrina* benthic $\delta^{18}O$ record to the global benthic $\delta^{18}O$ record (LR04 stack; Lisiecki & Raymo, 2005) to construct new tie points for an age model. We then did an independent check on the age model to assess the best one by comparing the benthic $\delta^{18}O$ record to the physical properties L* (sediment lightness) data from Site U1451A. The refined Site U1451A-23H/24H age model has an uncertainty of $\pm$20 kyr.

The average SST in the Southern Bay of Bengal did not change through the Pliocene-Pleistocene cooling (Figure 9). The stability of this region is in good agreement with other SST records in the IPWP (Wara et al., 2005; Dekens, unpublished; Table 2). We did see increased SST variability at Site U1451A from the Pliocene (~0.84°C) to the Pleistocene (~0.95°C) that is also shown in the ODP 758 record in the Northern Indian Ocean (Dekens, unpublished).

FUTURE WORK

Due to the closure of the SFSU and UCSC campuses related to the COVID-19 pandemic, we were unable to complete the analysis of all our samples. Sixteen *T. sacculifer* samples were picked, crushed, and cleaned for Mg/Ca measurement and await to be analyzed. This would have filled gaps in the SST record and increased the average sampling resolution from ~11 kyr to ~9 kyr. Additionally, the measurement of 98 *T. sacculifer* samples were split for $\delta^{18}O$ analysis. The

$\delta^{18}O$ analysis of *T. sacculifer* could provide an additional check on the age model by seeing if the peak glacials in the planktonic *T. sacculifer* record align with the peak glacials in the benthic *U. peregrina* record. Furthermore, the $\delta^{18}O$ of *T. sacculifer* could potentially be converted to $\delta^{18}O_{sw}$ to remove the effect of calcification temperature (Shackleton, 1974) and provide estimates of sea surface salinity.

REFERENCES

Anand, P., H. Elderfield, and M.H. Conte (2003), Calibration of Mg/Ca thermometry in planktonic foraminifera from a sediment trap time series, *Paleoceanography, 18(2)*, doi:10.1029/2002PA000846.

Barker, S., Greaves, M., & Elderfield, H. (2003). A study of cleaning procedures used for foraminiferal Mg/Ca paleothermometry. *Geochemistry, Geophysics, Geosystems*, *4*(9), 1–20.

Bemis, B.E., H.J. Spero, J. Bijma, and D.W. Lea (1998), Re-evaluation of the oxygen isotopic composition of planktonic foraminifera: Experimental results and revised temperature equations, *Paleoceanography, 13*, 150-160.

Boos, W.R., and Z. Kuang (2010), Dominant control of the South Asian monsoon orographic insulation versus plateau heating, *Nature, 463,* 218-223.

Boyle, E. A. (1983), Manganese carbonate overgrowths on foraminifera tests, *Geochim, Cosmochim. Acta, 47*, 1815-1819.

Brierley, C.M., A.V. Fedorov, Z. Liu, T.D. Herbert, K.T. Lawrence, and J.P. LaRiviere (2009), Greatly Expanded Tropical Warm Pool and Weakened Hadley Circulation in the Early Pliocene, *Science, 323,* 1714-1718.

Brierley, C.M., and A.V. Fedorov (2010), Relative importance of meridional and zonal sea surface temperature gradients for the onset of the ice ages and Pliocene-Pleistocene climate evolution, *Paleoceanography, 25,* PA2214, doi:10.1029/2009PA001809.

Broecker, W.S. and T.H. Peng (1982), Tracers in the Sea, *Eldigio Press, New York*, 1-690.

Brown, S. J., and H. Elderfield (1996), Variations in Mg/Ca and Sr/Ca of planktonic foraminifera caused by postdepositional dissolution: Evidence of shallow Mg-dependent dissolution, *Paleoceanography, 11,* 543-551.

Caley, T., B. Malaize, S. Zaragosi, L. Rossignol, and J. Bourget (2011), New Arabian Sea records help decipher orbital timing of Indo-Asian monsoon, *Earth Planet. Sci. Lett., 308*, 433-444.

Chen, J., J. W. Farrell, D. W. Murray, and W. L. Prell (1995), Timescale and paleoceanographic implications of a 3.6 m.y. oxygen isotope re- cord from the northeast Indian Ocean (Ocean Drilling Program Site 758), *Paleoceanography*, *10*, 21–47.

Clemens, S.C., Kuhnt, W., LeVay, L.J., and the Expedition 353 Scientists (2016), *Indian Monsoon Rainfall*. Proceedings of the International Ocean Discovery Program, 353: College Station, TX (International Ocean Discovery Program).

Clemens, S.C., W.L. Prell, and Y. Sun (2010), Orbital-scale timing and mechanisms driving Late Pleistocene Indo-Asian summer monsoons: reinterpreting cave speleothem d18O, *Paleoceanography, 25*, PA4207.

Curray, J.R., F.J. Emmel, D.G. Moore (2003), The Bengal Fan: morphology, geometry, stratigraphy, history and processes, *Mar. Pet. Geol., 19*, 1191-1223.

Dekens, P. S., D. W. Lea, D. K. Pak, and H. J. Spero (2002), Core top calibration of Mg/Ca in tropical foraminifera: Refining paleotemperature estimation, *Geochem. Geophys. Geosyst*., 3(4), 10.1029/2001GC000200.

Dekens, P.S., A.C. Ravelo, M.D. McCarthy, and C.A. Edwards (2008), A 5 million year comparison of Mg/Ca and alkenone paleothermometers, *Geochem. Geophys. Geosyst., 9,* Q10001, doi:10.1029/2007GC001931.

Duplessy, J.C., C. Lalou, and A.C. Vinot (1970), Differential isotopic fractionation in benthic foraminifera and paleotemperatures assessed, *Science, 168*, 250-251.

Emiliani, C. (1955), Mineralogical and chemical composition of the tests of certain pelagic foraminifera, *Micropaleontology, 1,* 377-380.

Fedorov, A.V., C.M. Brierley, K.T. Lawrence, Z. Liu, P.S. Dekens, and A.C. Ravelo (2013), Patterns and mechanisms of early Pliocene warmth, *Nature, 496,* doi:10.1038/nature12003.

France-Lanord, C., Spiess, V., Klaus, A., Schwenk, T., and the Expedition 354 Scientists (2016), *Proceedings of the International Ocean Discovery Program*, Volume 354, publications.iodp.org.

Gradstein, F.M., Ogg, J.G., Schmitz, M.D., and Ogg, G.M. (2012), *The Geological Time Scale* 2012: Amsterdam (Elsevier).

Hastings, D. W., A. D. Russell, and S. R. Emerson (1998), Foraminiferal magnesium in *Globeriginoides sacculifer* as a paleotemperature proxy, *Paleoceanography, 13,* 161-169.

Herbert, T., L. Peterson, K. Lawrence, and Z. Liu (2010), Tropical ocean temperatures over the past 3.5 million years, *Science, 328*, 1530-1534.

Hoogakker, B., H. Elderfield, K. Oliver, and S. Crowhurst (2010), Benthic foraminiferal oxygen isotope offsets over the last glacial-interglacial cycle, *Paleoceanography, 25*, PA4229, doi:10.1029/2009PA001870.

Jensen, T.G. (2003), Cross-equatorial pathways of salt and tracers from the northern Indian Ocean: Modelling results, *Deep Sea Res., Part II, 50*, 2111-2128.

Khan, M.H.R., J. Liu, S. Liu, A.A. Seddique, L. Cao, and A. Rahman (2019), Clay mineral compositions in surface sediments of the Ganges-Brahmaputra-Meghna river system of Bengal Basin, Bangladesh, *Mar. Geol., 412*, 27-36.

Kisakurek, B., A. Eisenhauer, F. Nohm, D. Garbe-Schonberg, and J. Erez (2008), Controls on shell Mg/Ca and Sr/Ca in cultured planktonic foraminiferan, *Globigerinoides ruber* (white), *Earth and Planetary Science Letter, 273*, 260-269.

Kleiven, H.F., E. Jansen, T. Fronval, and T.M. Smith (2002), Intensification of Northern Hemisphere glaciations in the circum Atlantic region (3.5-2.4 Ma) – ice-rafted detritus evidence, *Paleoceanography, Palaeoclimatology, Palaeocecology, 184,* 213-223.

Kolla, V., D.G. Moore, and J.R. Curray (1976), Recent bottom-current activity in the deep western Bay of Bengal, *Mar. Geol., 31*, 255-270.

Koziol, A.M. and R.C. Newton (1995), Experimental determination of the reactions magnesite plus quartz equals enstatite plus CO2 and magnesite equals periclase plus CO2, and enthalpies of formation of enstatite and magnesite, *American Mineralogist, 80*, 1252-1260.

Laskar, J., P. Robutel, F. Joutel, M. Gastineau, A.C.M Correia, and B. Levrard (2004), A long-term numerical solution for the insolation quantities of the Earth, *Astronomy & Astrophysics, 428,* 261-285.

Lawrence, K. T., Z. Liu, and T. D. Herbert (2006), Evolution of the Eastern Tropical Pacific through Plio-Pleistocene, *Science*, *312,* 79-83.

Lawrence, K. T., S. Sosdian, H. E. White, and Y. Rosenthal (2010), North Atlantic climate evolution through the Plio-Pleistocene climate transitions, *Earth and Planetary Science Letters, 300,* 329-342.

Lea, D. W., T. A. Mashiotta, and H. J. Spero (1999), Controls on magnesium and strontium uptake in planktonic foraminifera determined by live culturing, *Geochem. Cosmochim. Acta,* 63, 2369-2379.

Levitus, S. (1982). Climatological atlas of the world ocean. *US Government Printing Office, Washington DC*, *NOAA Profe*(13).

Li, C. and Yanai, M. (1996), The onset and interannual variability of the Asian summer monsoon in relation to land-sea thermal contrast, *J. Clim., 9*, 358-375.

Li Y., W. Han, W. Wang, M. Ravichandran, T. Lee, and T. Shinoda (2017), Bay of Bengal salinity stratification and Indian summer monsoon intraseasonal oscillation: 2. Impact on SST and convection, *J. Geophys. Res. Oceans,* 122, 4312-4328.

Lindzen, R.S., and S. Nigam (1987), On the role of sea surface temperature gradients in forcing low-level winds and convergence in the tropics. *J Atmos Sci, 44*, 2418-2436.

Lisiecki, L.E., and M.E. Raymo (2005), A Pliocene-Pleistocene stack of 57 globally distributed benthic d18O records, *Paleoceanography*, *20*, PA1003, doi:10.1029/2004PA001071.

Lisiecki, L.E., and M.E. Raymo (2007), Plio-Pleistocene climate evolution: trends and transitions in glacial cycle dynamics, *Quaternary Science Reviews, 26,* doi:10.1016/j.quascirev.2006.09.005.

Lisiecki, L.E., and J.V. Stern (2016), Regional and global benthic $\delta^{18}O$ stacks for the last glacial cycle, *Paleoceanography, 31*, 1368-1394.

Maslin, M.A., G.H. Haug, M. Sarnthein, and R. Tiedemann (1996), The progressive intensification of northern hemisphere glaciation as seen from the North Pacific, *Geol Rundsch, 85,* 452-465.

Medina-Elizalde, M., and D.W. Lea (2010), Late Pliocene equatorial Pacific, *Paleoceanography*, *25*, PA2208, doi:10.1029/2009PA001780.

Molnar, P., W.R. Boos, and D.D. Battisti (2010), Orographic controls on climate and paleoclimate of Asia: thermal and mechanical roles for the Tibetan Plateau, *Annu. Rev. Earth Planet. Sci., 38*, 77-102.

Nürnberg, D., J. Bijma, and C. Hemleben (1996), Assessing the reliability of magnesium in foraminiferal calcite as a proxy for water mass temperatures, *Geochim. Cosmochim. Acta, 60*, 803-814.

Regenberg, M., D. Nurnberg, S. Steph, J. Groeneveld, D. Garbe-Schonberg, R. Tiedemann, and W.-C. Dullo (2006), Assessing the effect of dissolution on planktonic foraminiferal Mg/Ca ratios: Evidence from Caribbean core tops, *Geochem. Geophys. Geosyst., 7,* Q07P15, doi:10.1029/2005GC001019.

Reilly, B.T., J.S. Stoner, P.A. Selkin, J.F. Savian, and L. Meynadier (2018), Data report: paleomagnetic directions from IODP Expedition 354, Hole U1451A, Cores 23H and 24H, *Proceedings of the International Ocean Discovery Program,* Volume 354.

Reilly, B. T., Bergmann, F., Weber, M. E., Stoner, J. S., Selkin, P., Meynadier, L., et al. (2020). Middle to Late Pleistocene Evolution of the Bengal Fan: Integrating Core and Seismic Observations for Chronostratigraphic Modeling of the IODP Expedition 354 8° North Transect. *Geochemistry, Geophysics, Geosystems*, *21*(4), e2019GC008878.

Roonwal, G.S., G.P. Glasby, and R. Chugh (1997), Mineralogy and geochemistry of surface sediments from the Bengal Fan, Indian Ocean, *J. of Asian Ear. Sci., 15*, 33-41.

Rosenthal, Y. and E.A. Boyle (1993), Factors controlling fluoride content of planktonic foraminifera: An evaluation of its paleoceanographic applicability, *Geochim, Cosmochim. Acta, 57,* 335-346.

Schott, F.A., and McCreary, J.P., Jr., 2001. The monsoon circulation of the Indian Ocean. *Progress in Oceanography,* 51(1):1–123.

Schott, F.A., Xie, S.-P., and McCreary, J.P., Jr., 2009. Indian Ocean circulation and climate variability. *Reviews of Geophysics,* 47(1):RG1002.

Seki, O., D.N. Schmidt, S. Schouten, E.C. Hopmans, J.S. Sinninghe Damste, and R.D. Pancost (2012), Paleoceanographic changes in the Eastern Equatorial Pacific over the last 10 Myr, *Paleoceanography, 27,* PA3224.

Shackleton, N. J. (1974), Attainment of isotopic equilibrium between ocean water and the benthonic foraminifera geuns Uvigerina: Isotopic changes in the ocean during the last glacial. *Colloques Internationaux Du C.N.R.S.*, *219*, 203–210.

Signh, S., S. Rai, S. Krishnaswami (2008), Sr and Nd isotopes in river sediments from the Ganga Basin: sediment provenance and spatial variability in physical erosion*, J. Geophys. Res., 113*, F03006.

St John, K.E.K., and L.A. Krissek (2002), The late Miocene to Pleistocene ice-rafting history of southeast Greenland, *Boreas*, 31, 28-35.

Wara, M. W., Ravelo, A. C., & Delaney, M. L. (2005). Climate change: Permanent El Niño-like conditions during the Pliocene warm period. *Science*, *309*(5735), 758–761. https://doi.org/10.1126/science.1112596.

Weber, M. E., and B. T. Reilly (2018), Hemipelagic and turbiditic deposits constrain lower Bengal Fan depositional history through Pleistocene climate, monsoon, and sea level transitions, *Quaternary Science Reviews, 199,* 159-173.

Weber, M.E., Wiedicke, M.H., Kudrass, H.R., Hunscher, C., and H. Erlenkeuser (1997), Active growth of the Bengal Fan during sea-level rise and highstand. *Geology, 25*, 315-318.

Weber, M.E., Wiedicke-Hombach, M., Kudrass, H.R., and H. Erlenkeuser (2003), Bengal Fan sediment transport activity and response to climate forcing inferred from sediment physical properties. *Sedimentary Geology, 155*, 361-381.

Weber, M.E., H. Lantzsch, P. Dekens, S.K. Das, B.T. Reilly, Y.M. Martos, C. Meyer-Jacob, S. Agrahari, A. Ekblad, J. Titschack, B. Holmes, P. Wolfgramm (2018), 200,000 years of monsoonal history recorded on the lower Bengal Fan – strong response to insolation forcing, *Global and Planetary Change, 166*, 107-119.

Zhisheng, A., Guoxiong, W., Jianping, L., Youbin, S., Yimin, L., Weijian, Z., … Juan, F. (2015), Global Monsoon Dynamics and Climate Change, *Annual Review of Earth and Planetary Sciences*, *43*(1), 29–77.

Ziegler, M., L.J. Lourens, E. Tuenter, F. Hilgen, G.J. Reichart (2010), Precession phasing offset between Indian summer monsoon and Arabian Sea productivity linked to changes in Atlantic overturning circulation, *Paleoceanography, 25,* PA3213.

APPENDICES

Appendix 1 – Alternative Age Models

Constructing accurate age models in the Bengal Fan come with challenges due to its depositional environment and limited recovery. Calcareous nannofossils, planktonic foraminifers, and geomagnetic reversals were identified at Site U1451A and used to construct a preliminary age model (Figure A1.1; France-Lanord et al., 2016). To convert the age-depth relationship of sections 23H and 24H at Site U1451A, we initially used the reversals of the lower Cobb Mountain (1.185 Ma, 83.44 m), the Gauss-Matuyama (2.58 Ma, 130.60 m), and the Gauss-Gilbert-Gauss Chron boundary (3.596 Ma, 143.00 m) to construct an age model (Figure A1.2; France-Lanord et al., 2016; Reilly et al., 2018). An additional reversal identified but not interpreted on ship can now be interpreted as the upper Olduvai boundary (1.778 Ma, 108.30 m) since the Gauss-Matuyama boundary was identified (Reilly et al., 2018). Only the Gauss-Matuyama is identified in the depth range of Cores 23H and 24H (121-138 m), but the single polarity in each core suggests the studied interval must be older than 1.945 Ma and younger than 3.032 Ma (Reilly et al., 2018). Long-term sedimentation rates using the upper Olduvai, Gauss-Matuyama, and Gilbert-Gauss tie points for Cores 23H and 24H were 2.78 cm/ka and 1.22 cm/ka, respectively. The cores have similar hemipelagic lithologies which suggests that they should have similar sedimentation rates. The preliminary age model for Site U1451A needed refining based on the tie points used from the reversals were located outside of Cores 23H and 24H and did not provide an accurate age-depth relationship for Site U1451A-23H/24H.

A refined age model for Site U1451A was developed using the $\delta^{18}O$ analysis of the benthic species *U. peregrina*. Three age models were developed (Figure 6, Figure A1.3, Figure A1.4) using the method described in the results section, *Site U1451A Age Model*. The age model with the most extreme sedimentation rates is shown in Figure A1.3. This age model (Figure A1.3) does not agree well with the independent obliquity check using the physical properties data for sediment lightness. The age models from Figure A1.4 and Figure 6 have similar sedimentation rates between tie points, but the age model from Figure 6 agrees most with the independent obliquity check using the physical properties data for sediment lightness from Site U1451A and was selected as the age model for Site U1451A, Cores 23H and 24H. Further work on the age model can improve it by increasing the sampling resolution for the benthic $\delta^{18}O$ record. 6 cm for each of the 130 samples were left untouched and have the potential to find more *U. peregrina* to increase the resolution in the $\delta^{18}O$ record. A higher resolution $\delta^{18}O$ record would ideally decrease the age uncertainty in the age model.

TABLES

Pliocene-Pleistocene Age Model

Site	Core	Depth CSF-A (m)	Age (ka)	Sedimentation Rate (cm/ka)	Stratigraphic Tie Point
U1451A	23H	121.62	2098.00		
U1451A	23H	122.92	2140.00	3.06	
U1451A	23H	124.66	2260.00	1.45	
U1451A	23H	129.66	2548.00	1.74	
U1451A	23H/24H	130.60	2580.00	2.89	Gauss/Matuyama
U1451A	24H	133.52	2770.00	1.54	
U1451A	24H	135.93	2898.00	1.89	
U1451A	24H	137.92	3000.00	1.94	
		Average Sedimentation Rate		2.07	

Table 1. The table shows the Site U1451A-23H/24H age model's tie points with the depth-age relationship. The average sedimentation rate is 2.07 cm/ka. The Gauss-Matuyama reversal is the one magnetic reversal seen in these cores (dated at 2580.00 ka; Reilly et al., 2018).

Pliocene-Pleistocene Tropical SST

Site	Location	Range (°C)	Mean (°C)	Avg Resolution (ka)
IODP 1451A	S. Bay of Bengal	26.6-30.9	28.6	11.6
ODP 758	N. Indian Ocean	25.1-30.8	28.0	15.3
ODP 806	W. Eq. Pacific	25.0-31.5	28.5	7.9
ODP 847	E. Eq. Pacific	22.8-29.4	26.6	18.1

Table 2. A table comparing IODP site U1451A to Mg/Ca SST from the tropics from ~2.1-3.0 Ma. The range, mean, and average sampling resolution are given for IODP Site U1451A (this study), ODP Site 758 (Dekens, unpublished), ODP Site 806 (Wara et al., 2005), and ODP site 847 (Wara et al., 2005).

FIGURES

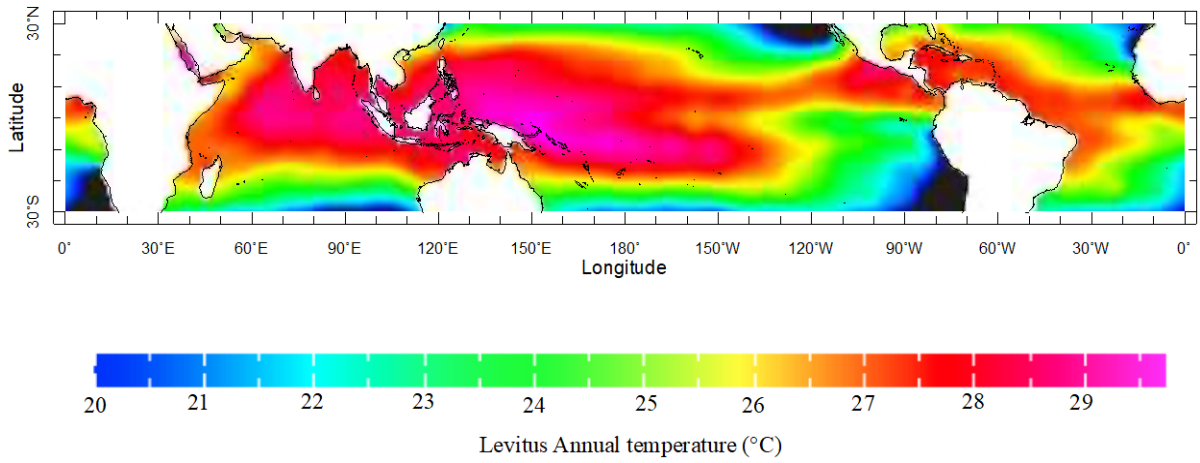

Figure 1. Modern SST map of tropical and subtropical regions from 30°S to 30°N (Levitus, 1982). Site U1451A is located at 8°N, 88°E. The temperature range (°C) is shown in the legend.

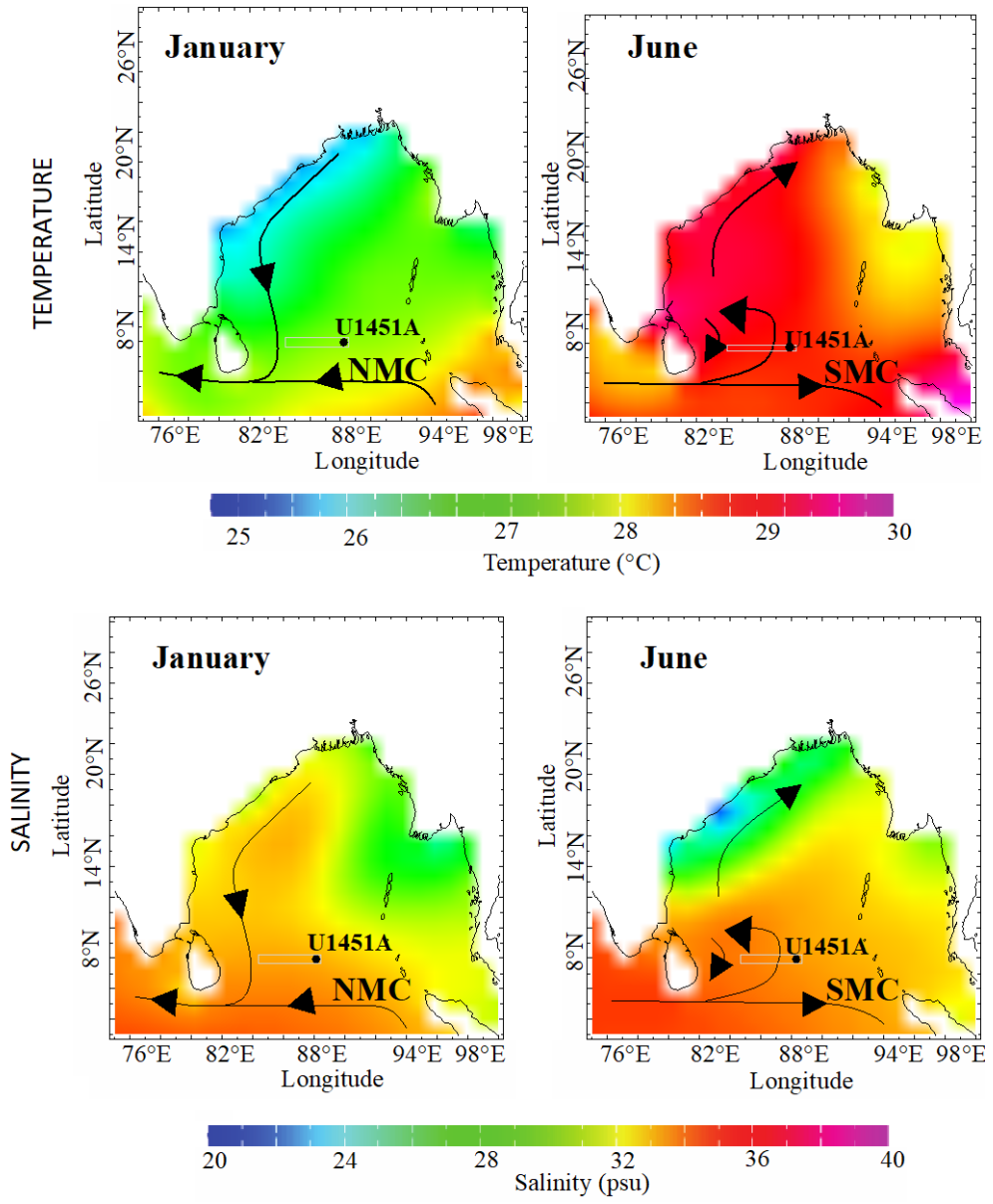

Figure 2. Modern SST and SSS maps of the Bay of Bengal for January and June (Levitus, 1982). The reversal of surface currents is shown with the Northeast Monsoon Current (NMC) flowing southward in January and the Southwest Monsoon Current (SMC) flowing northward in June.

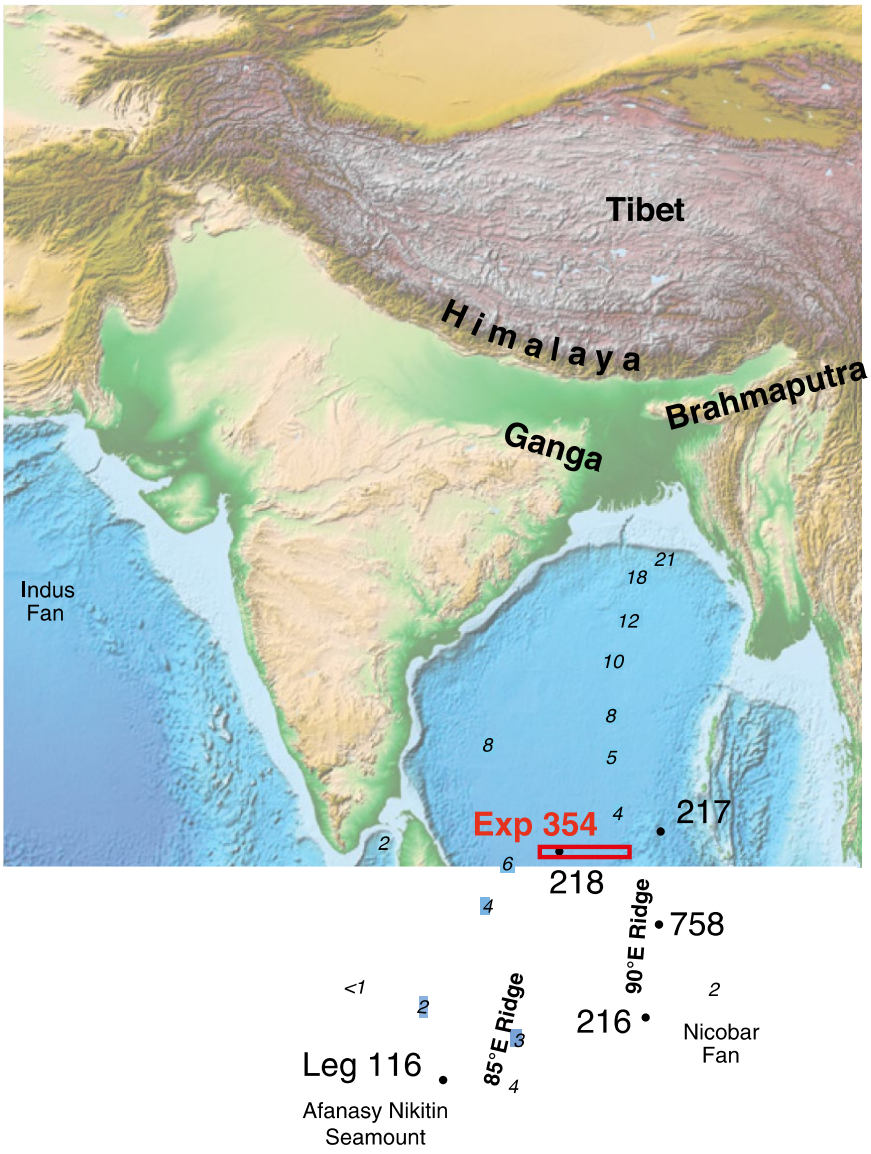

Figure 3. A map of the greater Bay of Bengal region with a red box around where International Ocean Discovery Program (IODP) Expedition 354 drilled the seven-site east-west transect at 8°N in the Southern Bay of Bengal.

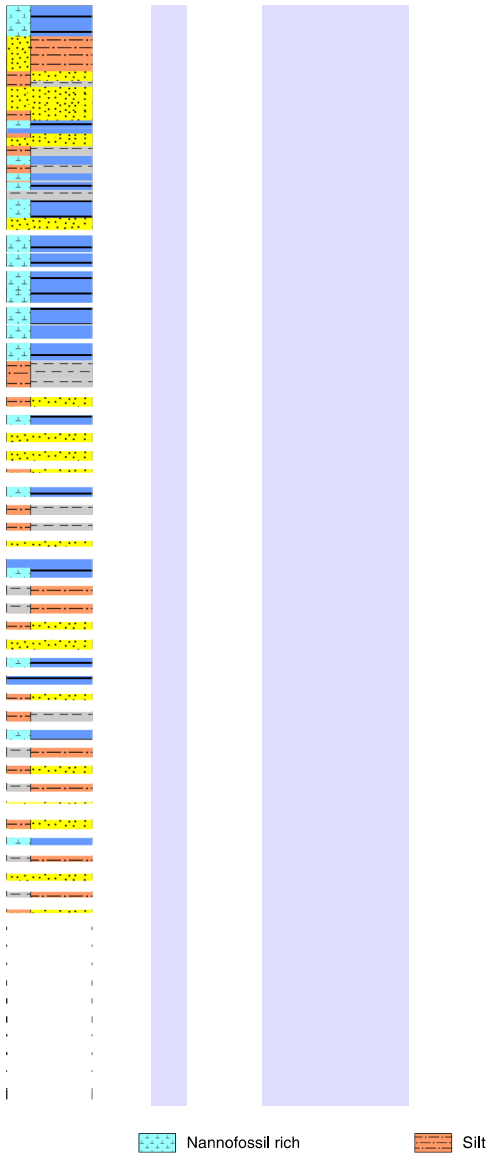

Figure 4. The graphic lithologies of the cores of Hole U1451A are shown along with the core recovery, and maximum grain size for the first 580 mbsf (France-Lanord et al., 2016).

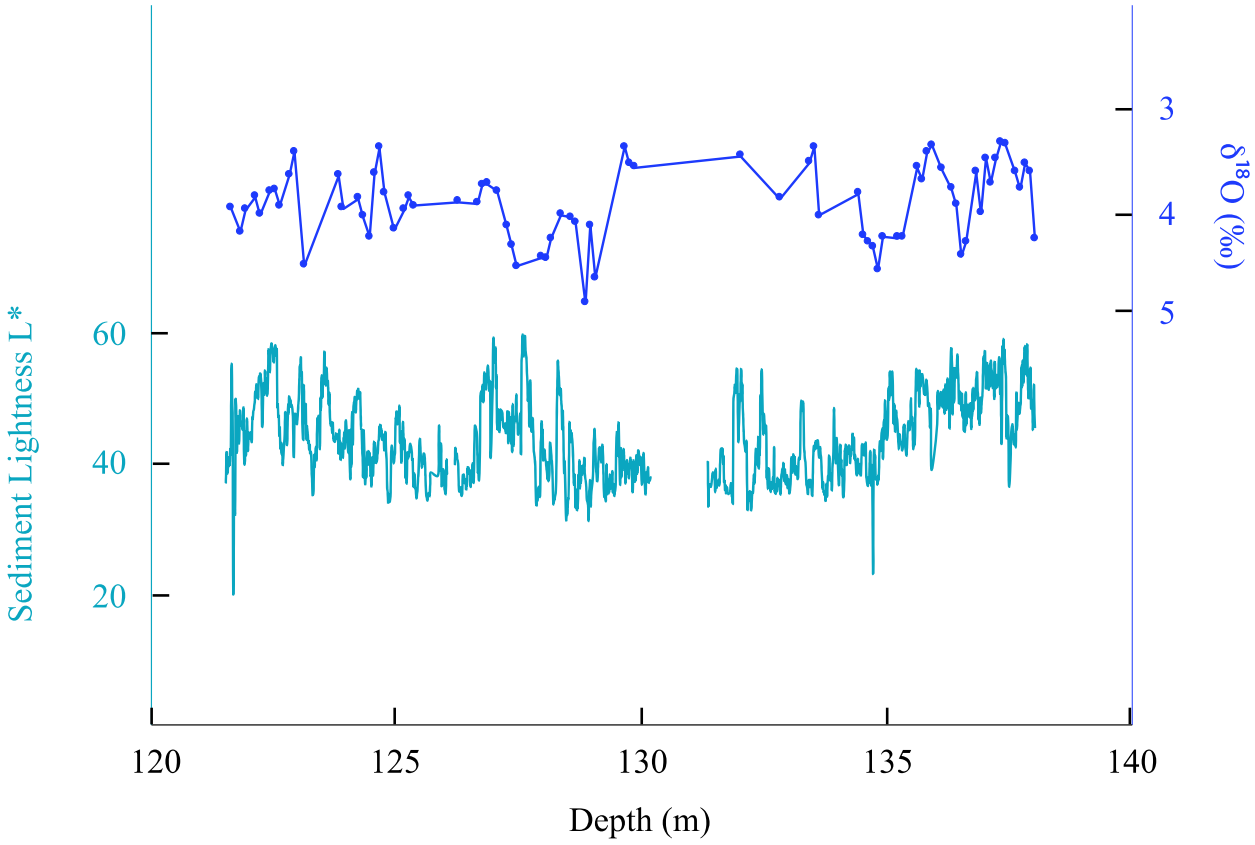

Figure 5. The $\delta^{18}O$ (‰) of the benthic species *U. peregrina* at Site U1451A is shown (dark blue line) vs depth below seafloor (m) at Site U1451A. The sediment lightness L* data at Site U1451A is shown (light blue line) vs depth below seafloor (m).

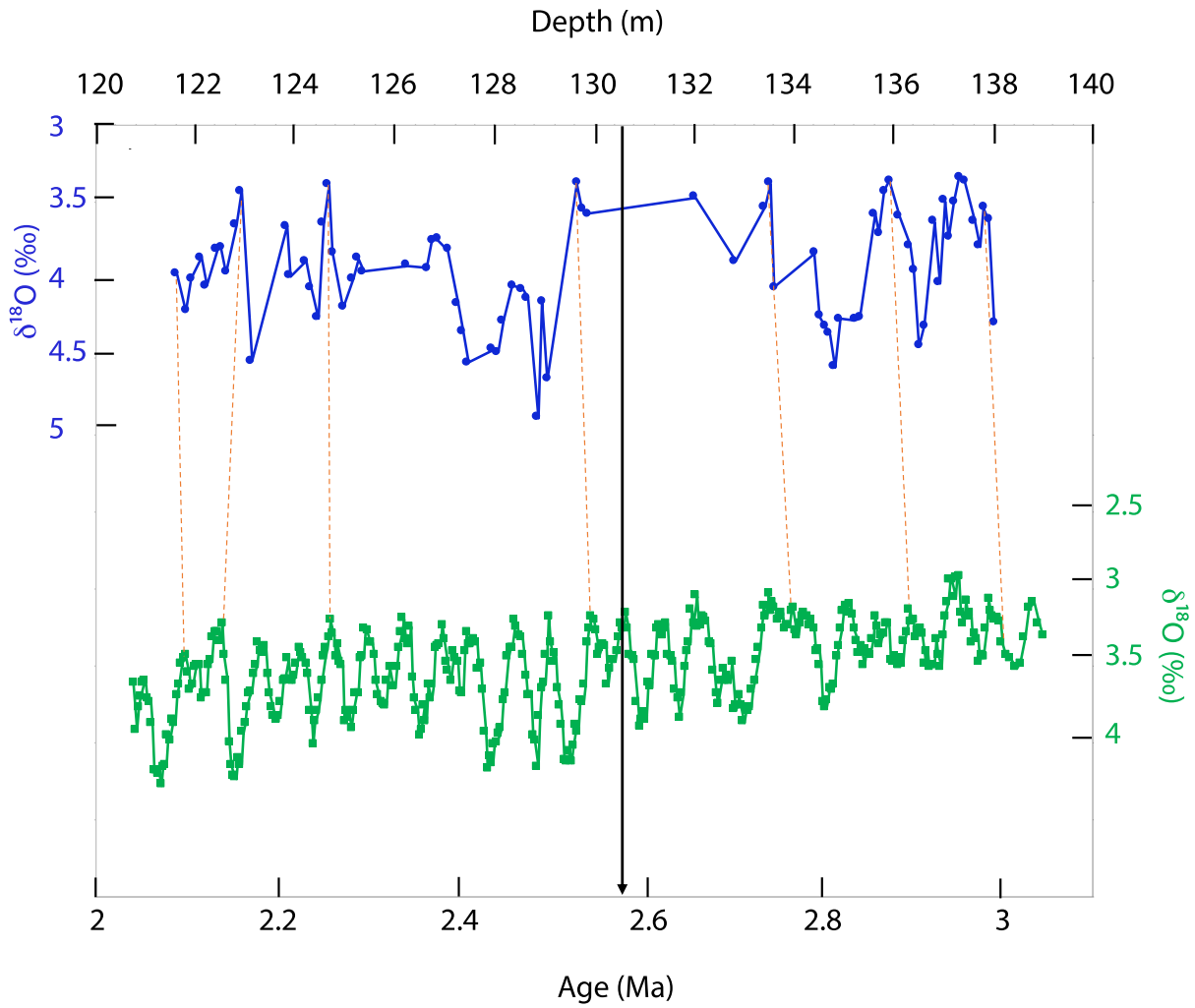

Figure 6. The age model for Site U1451A was constructed using the benthic $\delta^{18}O$ stable isotope record of *U. peregrina* at Site U1451A (blue line) and comparing it the global benthic LR04 stack (green line) (Lisiecki & Raymo, 2005). The tie points used to align the site U1451A $\delta^{18}O$ record on depth (m) to the LR04 record for age (Ma) (Lisiecki & Raymo, 2005) are shown with the orange dashed lines. The black line represents the Gauss-Matuyama magnetic reversal at 130.6 m and 2.58 Ma (Reilly et al., 2018).

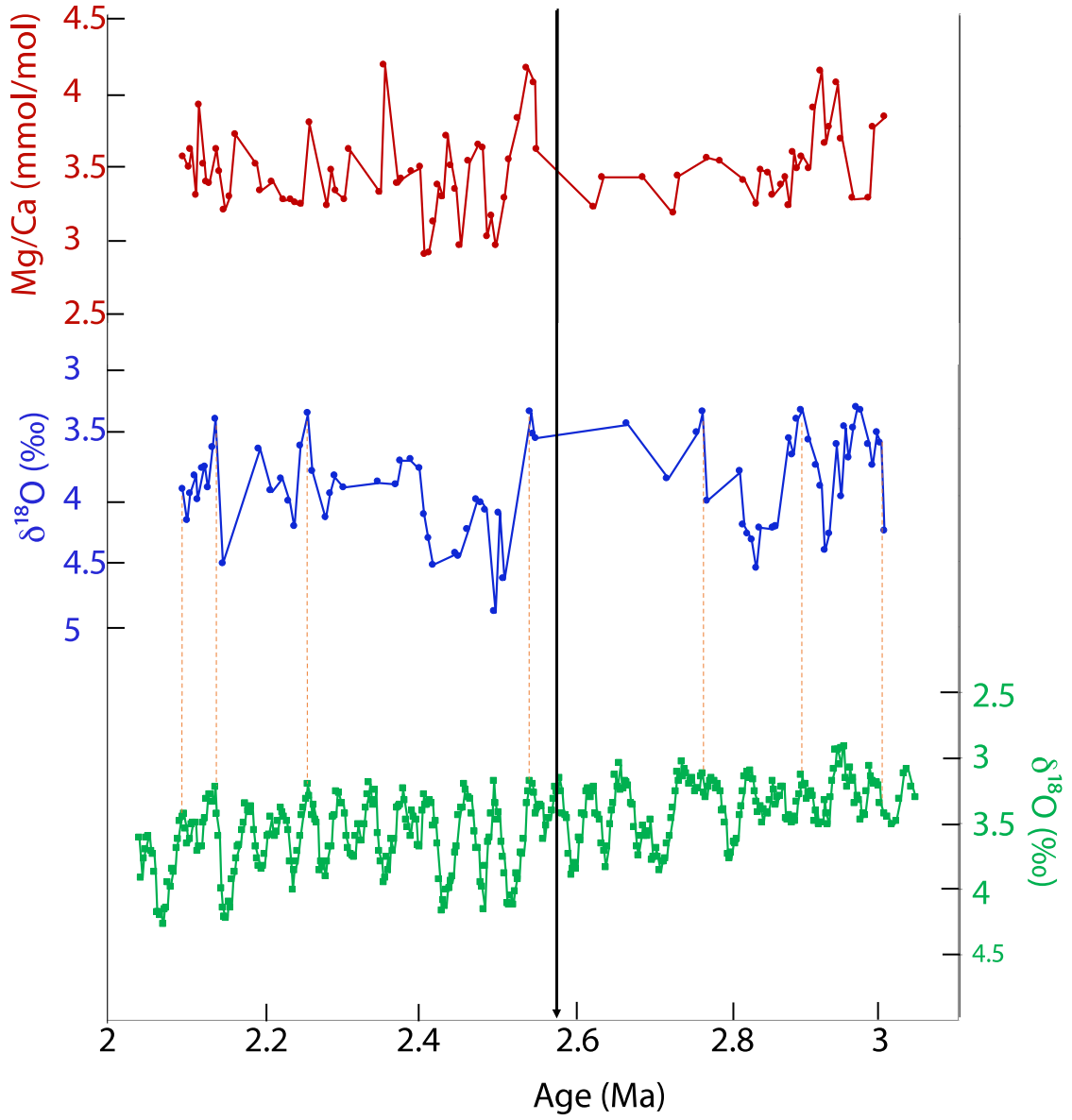

Figure 7. The U1451A age model was applied to convert depth (m) to age (Ma) for the *U. peregrina* $\delta^{18}O$ record at the site (blue line) and the Mg/Ca (mmol/mol) of *T. sacculifer* (red line). The alignment of site U1451A benthic $\delta^{18}O$ record to the LR04 stack (Lisiecki& Raymo, 2005) is shown with the orange dashed lines. The black line represents the Gauss-Matuyama magnetic reversal dated at 2.58 Ma (Reilly et al., 2018).

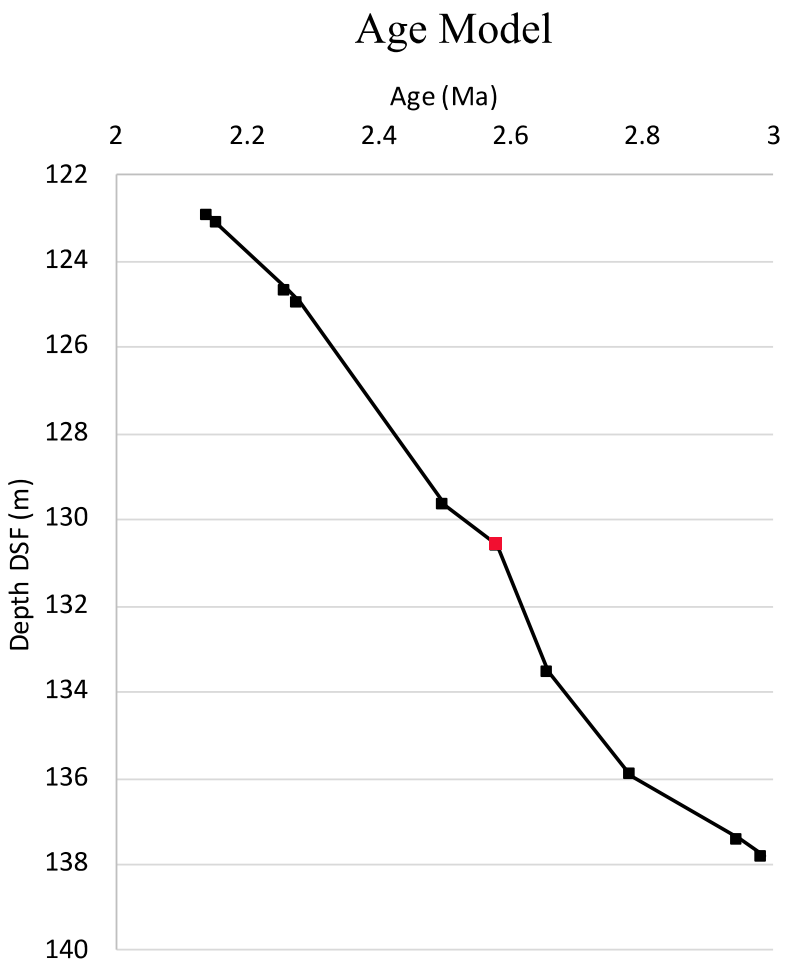

Figure 8. Site U1451A's benthic $\delta^{18}O$ record was used to construct the site's age model. The black squares represent the stratigraphic tie points that were constructed by comparison of site U1451A's benthic $\delta^{18}O$ record to the LR04 benthic $\delta^{18}O$ record (Lisiecki & Raymo, 2005). The red square represents the Gauss-Matuyama magnetic reversal at 130.6 DSF (m) and 2.58 Ma.

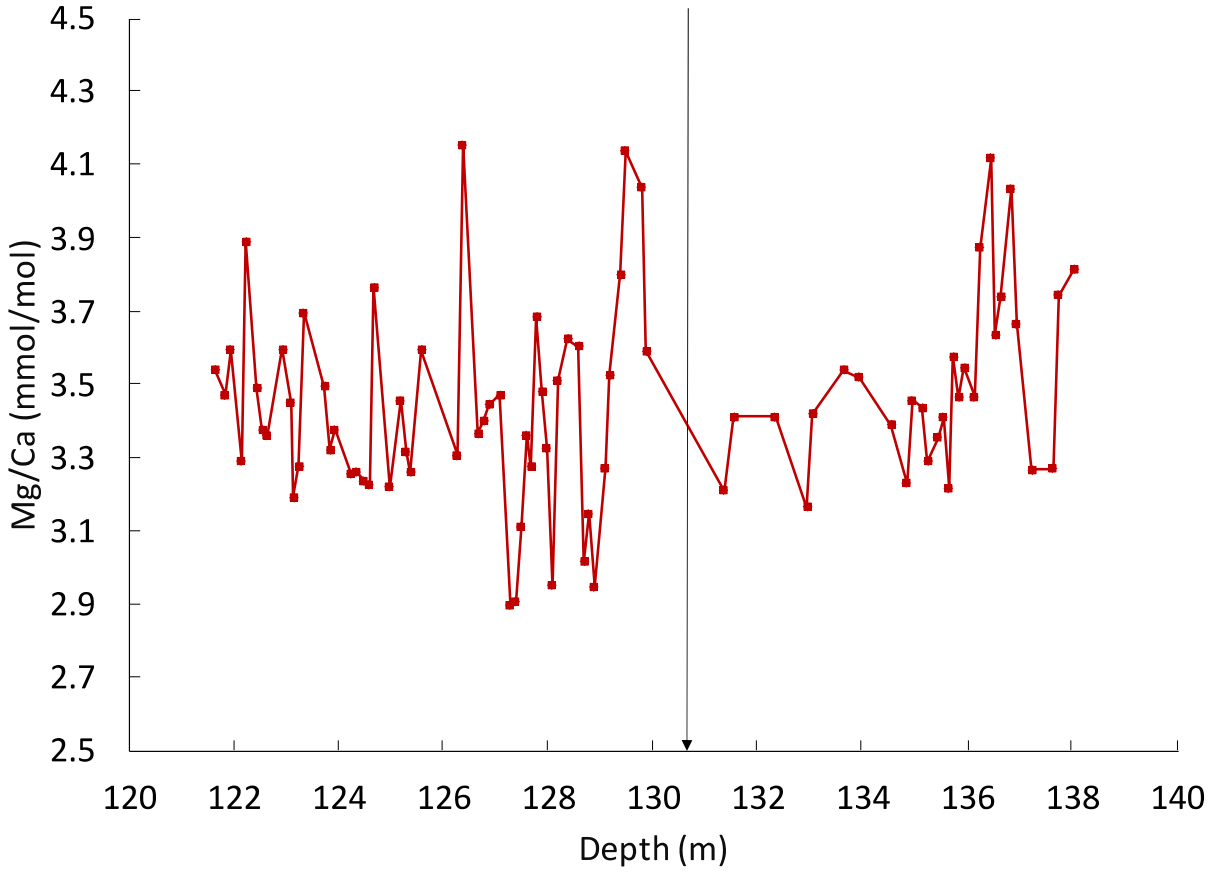

Figure 9. Mg/Ca (mmol/mol) of *T. sacculifer* at Site U1451A is plotted vs DSF (m). The black line represents the Gauss-Matuyama magnetic reversal at 130.6 DSF (m).

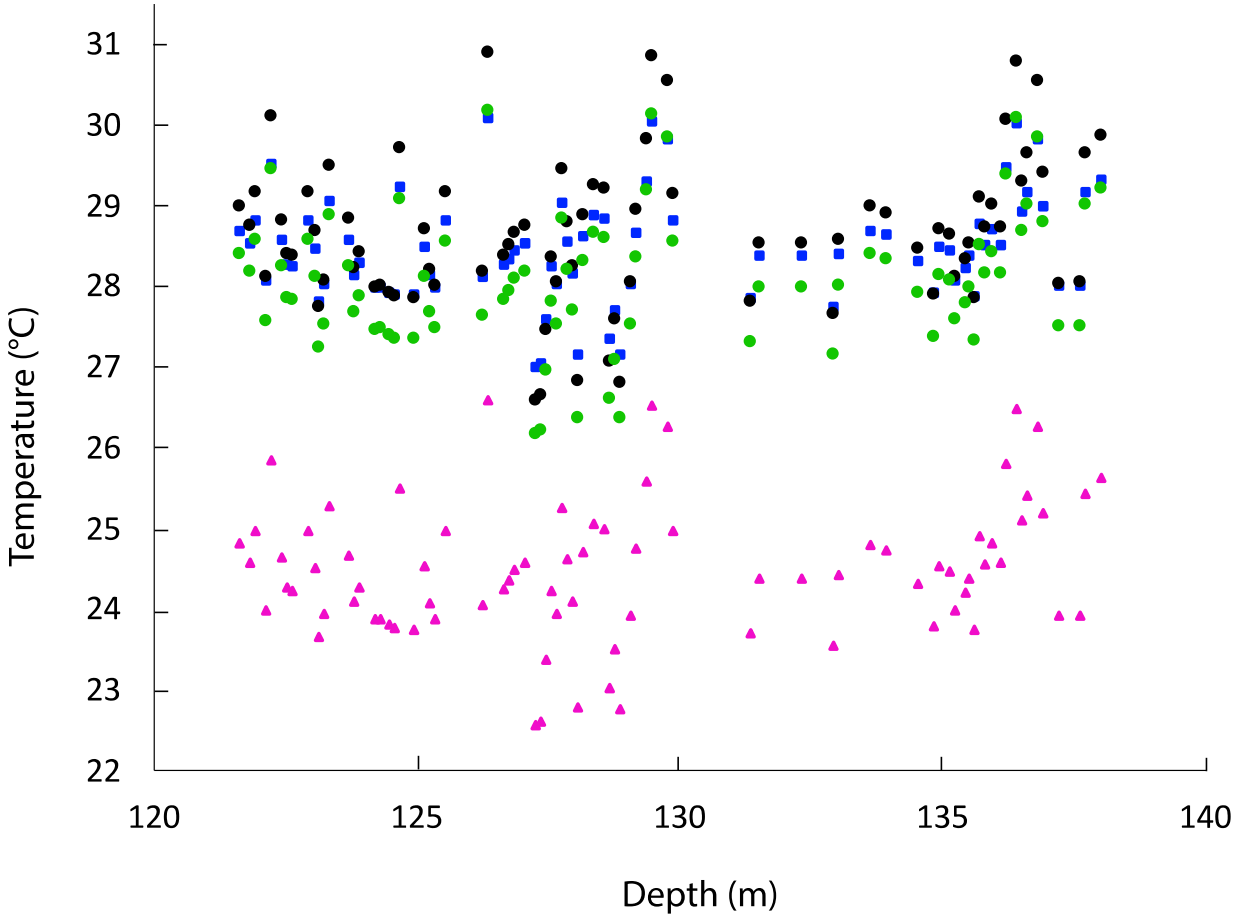

Figure 10. SST calibrations used to convert Mg/Ca of *T. sacculifer* to sea surface temperature (°C) vs age (Ma). The pink triangle uses Anand et al., 2003 calibration with B = 0.38. The blue square uses the Regenberg et al., 2006 dissolution correction with the Anand et al., 2003 calibration with B = 0.347. The green circle uses the Dekens et al., 2002 depth correction. The black circle uses the Dekens et al., 2002 ΔCO_3^{2-} correction.

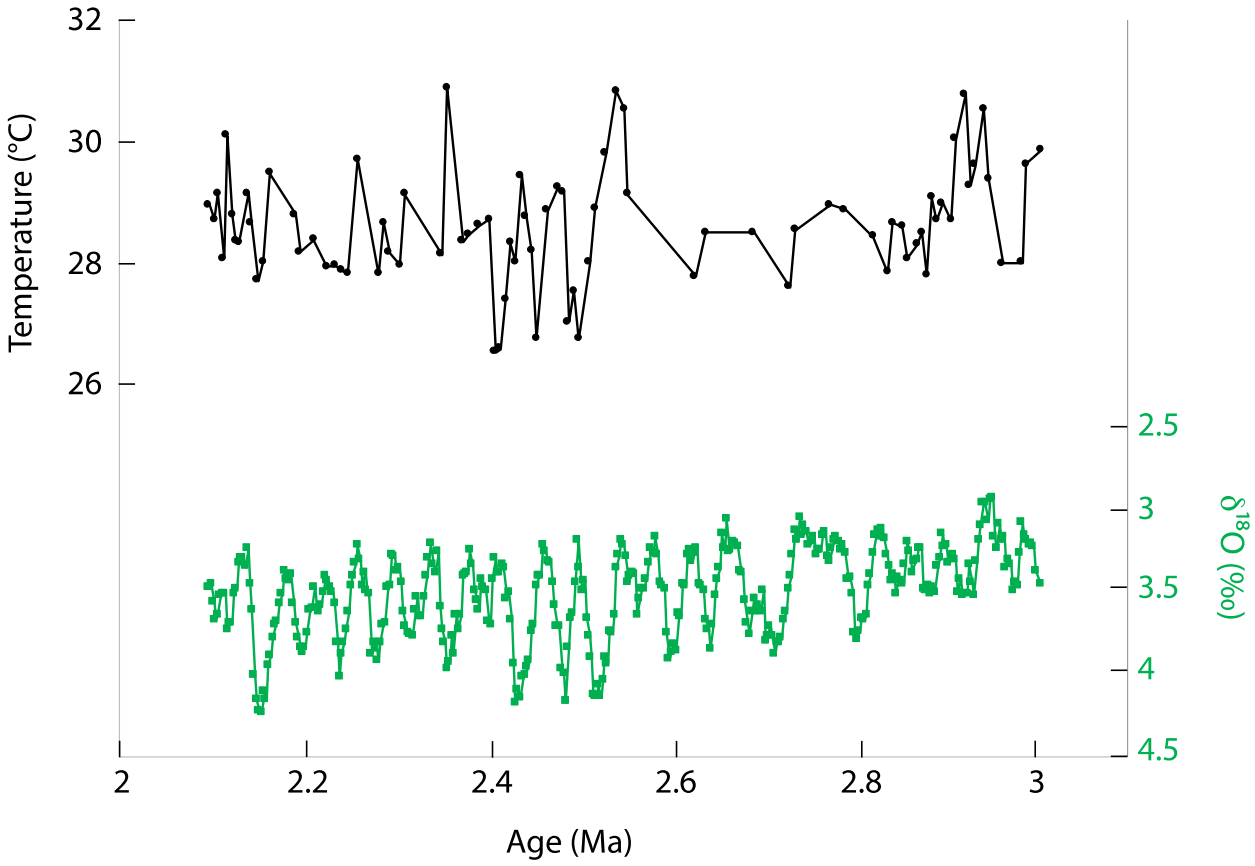

Figure 11. The selected calibration to represent SST at Site U1451A (black line) corrects for dissolution using the ΔCO_3^{2-} ion (Dekens et al., 2002). The LR04 stack (Lisiecki & Raymo, 2005) is plotted below (green line) for the age range produced from the Site U1451A age model.

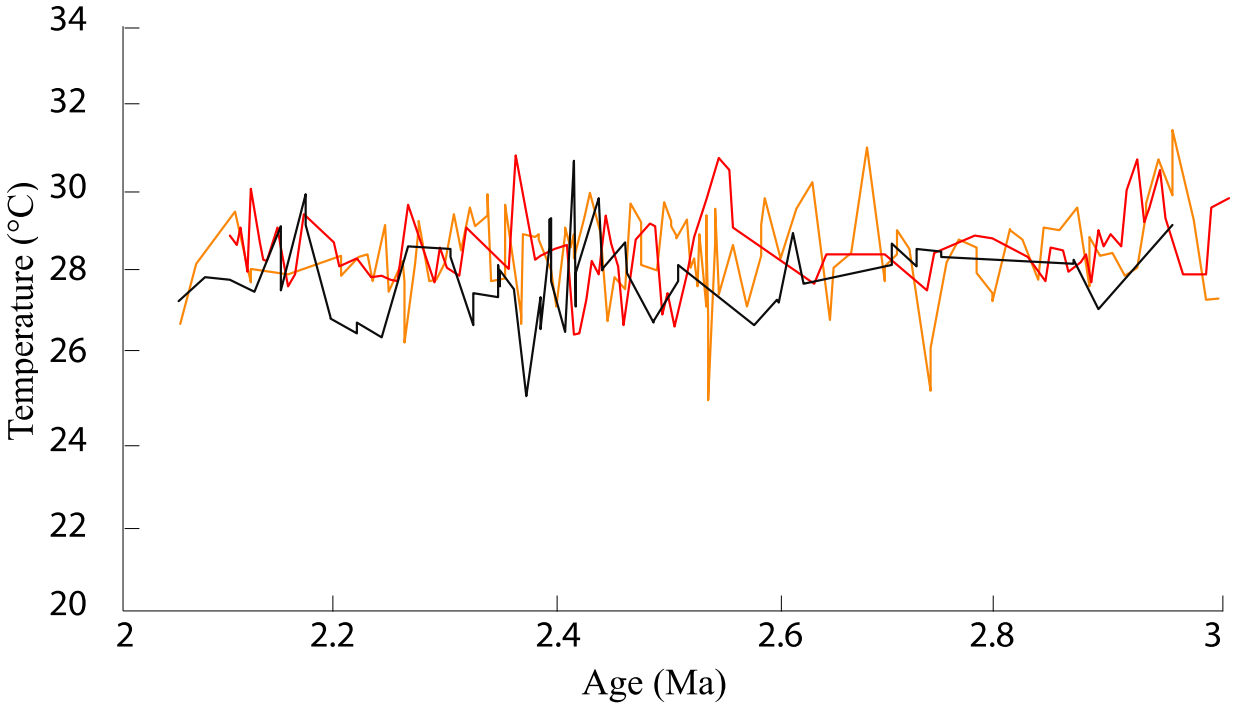

Figure 12. A comparison of Site U1451A SST (black line; this study) in the Southern Bay of Bengal with other records in the IPWP, Site 758 (orange line; Dekens, unpublished) and Site 806 (red line; Wara et al., 2005). These records show no cooling trend through the Pliocene-Pleistocene transition.

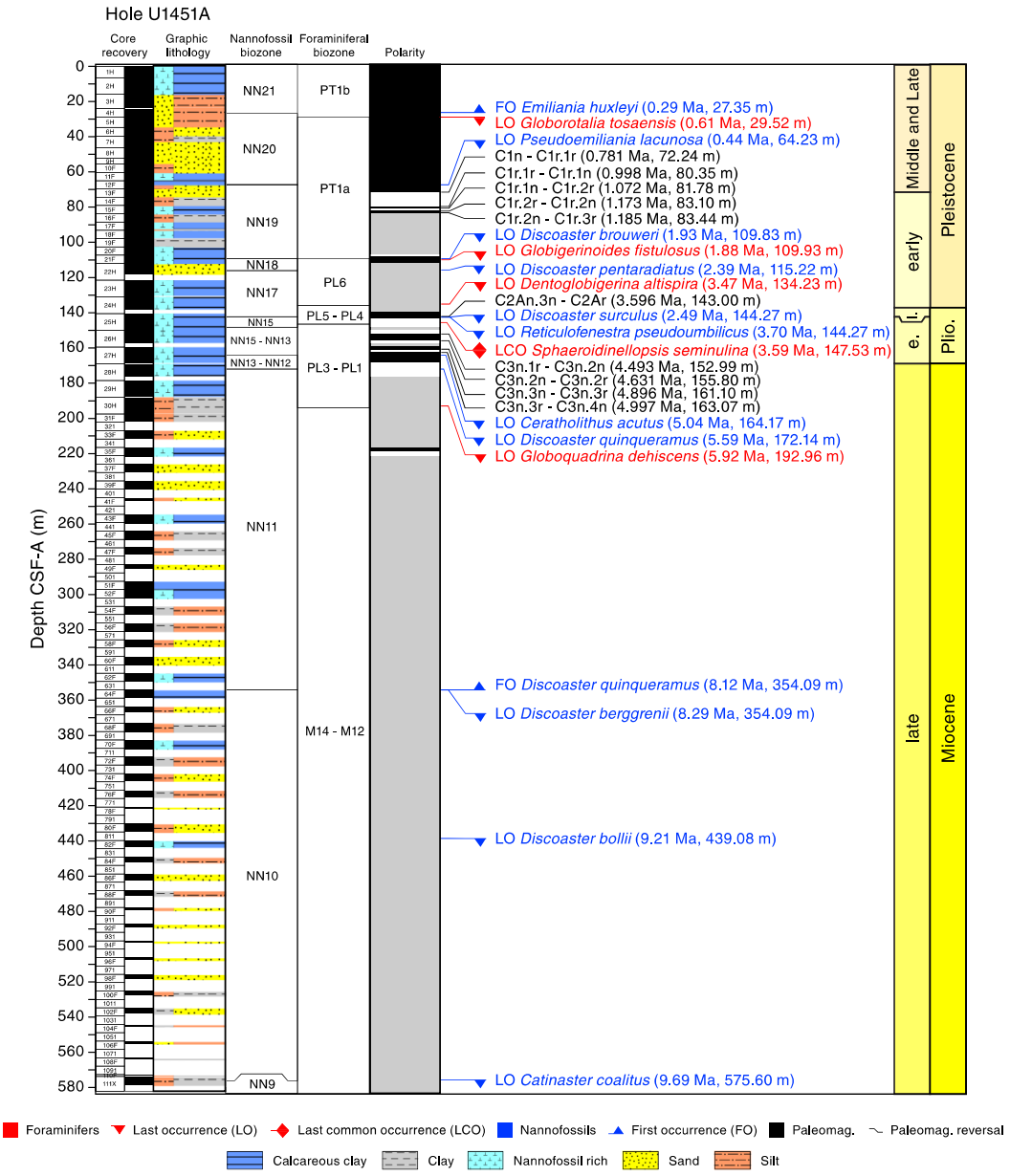

Figure 13 The preliminary age model from Site U1451A is shown. The magnetic reversals are shown in black and were used to construct the preliminary age model (Figure A1.2).

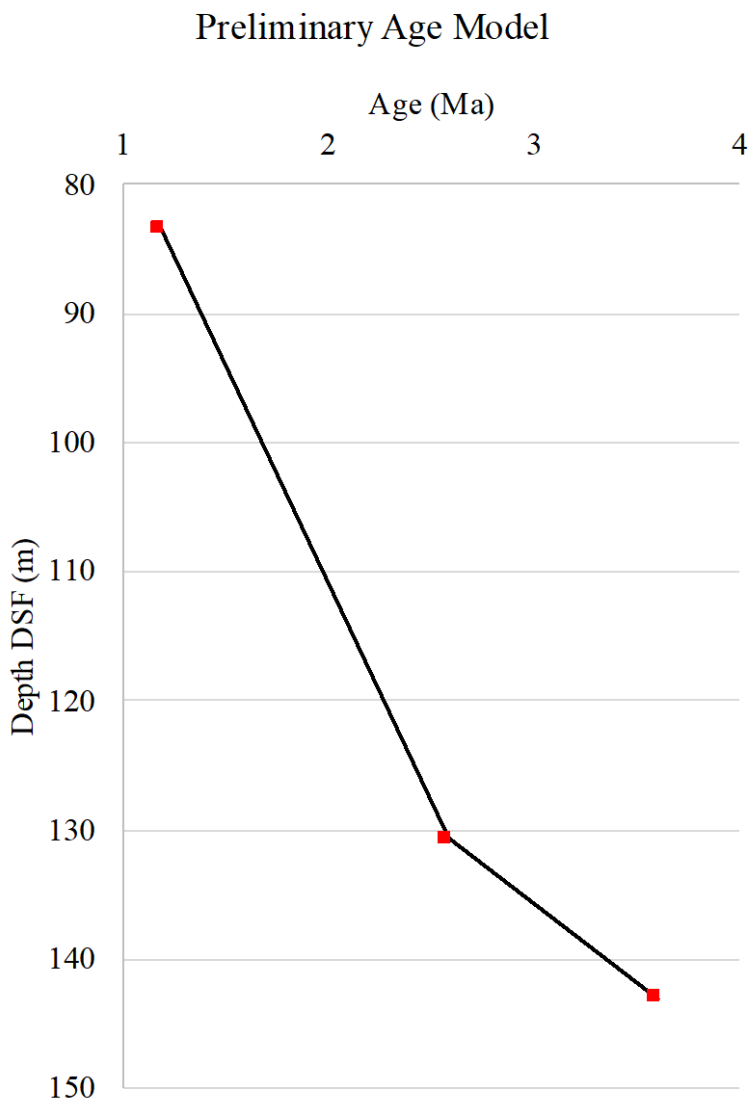

Figure A1.2. The preliminary age-depth relationship for the age model that used the Lower Cobb Mountain reversal, the Gauss-Matuyama reversal, and the Gauss-Gilbert reversal as tie points.

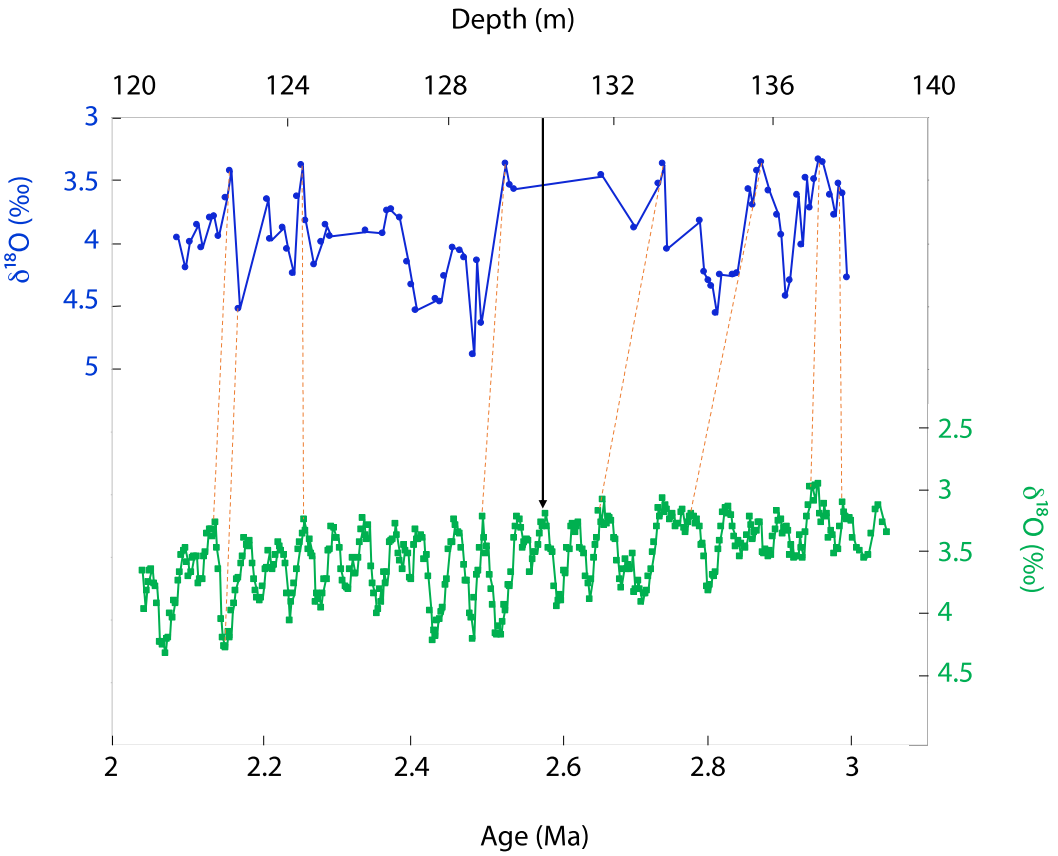

Figure A1.3. An age model for Site U1451A-23H/24H that compared the benthic $\delta^{18}O$ of *U. peregrina* (blue line) to the global benthic $\delta^{18}O$ record (green line; LR04 stack; Lisiecki & Raymo, 2005). The black line represents the Gauss-Matuyama magnetic reversal at 2.58 Ma (Reilly et al., 2018).

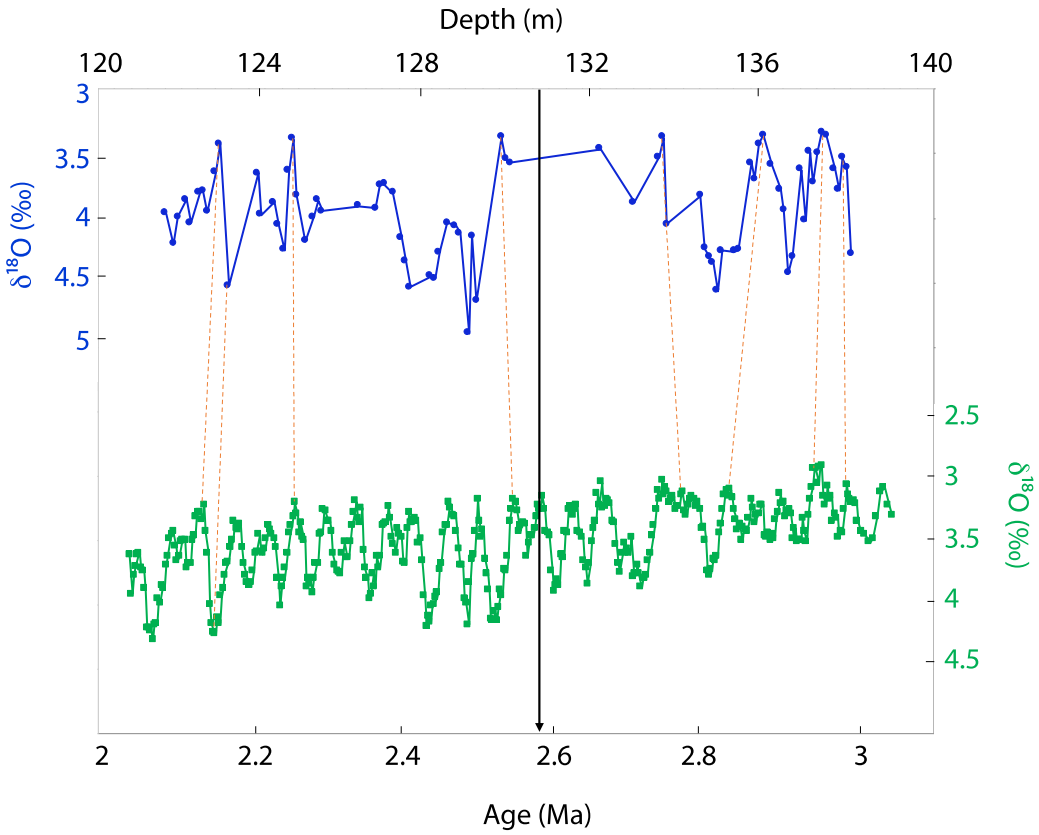

Figure A1.4. An age model for Site U1451A-23H/24H that compared the benthic $\delta^{18}O$ of *U. peregrina* (blue line) to the global benthic $\delta^{18}O$ record (green line; LR04 stack; Lisiecki & Raymo, 2005). The black line represents the Gauss-Matuyama magnetic reversal at 2.58 Ma (Reilly et al., 2018).